Type 2 Diabetes: One Disease, Many Pathways

Joon Ha

Arthur Sherman

Laboratory of Biological Modeling

National Institutes of Health

Bethesda, MD USA

Abstract (249 words)

Diabetes is a chronic, progressive disease that calls for longitudinal data and analysis. We introduce a longitudinal mathematical model that is capable of representing the metabolic state of an individual at any point in time during their progression from normal glucose tolerance to type 2 diabetes (T2D) over a period of years. As an application of the model, we account for the diversity of pathways typically followed, focusing on two extreme alternatives, one that goes through impaired fasting glucose (IFG) first, and one that goes through impaired glucose tolerance (IGT) first. These two pathways are widely recognized to stem from distinct metabolic abnormalities in hepatic glucose production and peripheral glucose uptake, respectively. We confirm this but go beyond to show that IFG and IGT lie on a continuum ranging from high hepatic insulin resistance and low peripheral insulin resistance to low hepatic resistance and high peripheral resistance. We show that IFG generally incurs IGT, and IGT generally incurs IFG on the way to T2D, highlighting the difference between innate and acquired defects and the need to assess patients early to determine their underlying primary impairment and appropriately target therapy. We also consider other mechanisms, showing that IFG can result from impaired insulin secretion, that non-insulin dependent glucose uptake can also mediate or interact with these pathways, and that impaired incretin signaling can accelerate T2D progression. We consider whether hyperinsulinemia can cause insulin resistance in addition to being a response to it and suggest that this is a minor effect.

Introduction

Diabetes is by definition a state of hyperglycemia, but its natural history is diverse. For example, some individuals experience fasting hyperglycemia first (Impaired Fasting Glucose, IFG), followed by hyperglycemia at the two-hour time point (2hPG) of an oral glucose tolerance test (OGTT), defined as Impaired Glucose Tolerance (IGT), and some experience these in the opposite order. Eventually, all people with diabetes will have both IFG and IGT (combined glucose impairment, CGI), so we refer to these two pathways as "IGT-first" and "IFG-first", respectively. An important implication of these observations is that the best period for determining differences in the underlying physiology of these pathways is during the pre-diabetic stage, when the phenotypes are still distinct.

Prediabetes is also the stage in which progression to type 2 diabetes (T2D) can be markedly delayed or prevented (45), and interventions can plausibly be made even more effective by targeting the specific metabolic defects of the patient. For example, IFG is generally thought to reflect insulin resistance at the liver, resulting in elevated hepatic glucose production (HGP), whereas IGT is thought to reflect peripheral insulin resistance, mainly in muscle, resulting in reduced glucose disposal. One would like to know whether using drugs that primarily affect hepatic or peripheral insulin resistance makes a material difference for patients on the IFG-first or IGT-first pathways, and whether any such benefit carries over once T2D has begun.

Moreover, diabetes is not a state that one enters and exits, like an infection, but a chronic condition that is the culmination of a series of gradual changes. Understanding of this progression is best obtained by longitudinal studies over a period of years or decades. Here we will focus on one such study, the Baltimore Longitudinal Study of Aging (BLSA) (51), which asked whether CGI is an obligatory stage

between IFG and T2D and between IGT and T2D (Supplemental Fig. S1; all supplemental material is available at Figshare, https://doi.org/10.6084/m9.figshare.10792412).

These features of diabetes suggest that a longitudinal mathematical model for disease progression could be a valuable adjunct to clinical studies. Here we establish such a model and demonstrate that it can distinguish hepatic and peripheral insulin resistance and can simulate the IGT-first and IFG-first pathways to T2D over a period of years. We will use the model to address the clinical questions raised by the BLSA and Perrault studies. By tracking virtual patients continuously in time, the model can interpolate between clinical observations, which are necessarily sparsely sampled, and indicate what is likely to have happened in the interim.

The model provides broader insight into the different insulin-resistance phenotypes, showing that a wide array of pathways, ranging from isolated IFG to isolated IGT to combinations of the two, can be obtained by combining different degrees of hepatic and peripheral insulin resistance. Thus, the apparent clinical diversity of individual paths comprises a set of quantitative variants within a unified process of metabolic dysfunction.

There is also diversity in the relative contributions of insulin resistance and beta-cell dysfunction to diabetes pathogenesis. This is particularly apparent in comparing diabetes risk factors in populations with a high prevalence of obesity, such as those of African descent and Native Americans, to populations in which diabetes risk is seen among lean individuals and beta-cell function is weaker, such as South and East Asians; populations of European descent tend to lie in between (46). Furthermore, beta-cell dysfunction can be subdivided into defects in first- and second-phase insulin secretion. As a first installment on this large and complex set of problems, we examine whether the loss of first-phase secretion early in pre-diabetes plays a fundamental causal role in T2D development or is just a useful marker.

General modeling approach

The diabetes field is fortunate to have a strong tradition of mathematical modeling (20, 49). A common feature of those models is that they provide snapshots in time of the metabolic state of an individual, including insulin resistance and beta-cell function. These models have been used to track progression by taking a series of snapshots, but they do not contain mechanisms of progression and do not describe trajectories of progression.

The model developed here belongs to a different family of models that seek to explain disease progression mechanistically, rather than assess the current state. It is an extension of our previously published model of beta-cell mass and function, which successfully simulated progression to diabetes in rodents over months and humans over years (37). That model, in turn, was based on the seminal model of (75), which expressed mathematically the hypothesis that beta-cell mass provides negative feedback on a slow time scale to compensate for insulin resistance. If that compensation is inadequate, however, the toxic effects of very high glucose overcome the stimulatory effects of moderately elevated glucose. The normal homeostatic negative feedback is converted to positive feedback, leading to deterioration in glucose tolerance and culminating in diabetes. This fundamental concept has been incorporated into other models that broadly agree but emphasize different details (23, 24, 35, 38, 43, 79). Notably, the model of (38) was shown to be able to account for the progression of fasting hyperglycemia and T2D observed in the Diabetes Prevention Program (DPP)(45).

A third class of modeling studies has fit longitudinal data from clinical studies with non-linear mixed effects statistical approaches to assess the magnitude of treatment effects on glucose, insulin and HbA1c (18, 25) or, by fitting to a modified form of the model of (75), on beta-cell mass and insulin sensitivity (67).

103 See (24) for further comment on the models cited here and other models, and see (54) for a perspective on
104 modeling T2D.
105 The initial wave of mechanistic longitudinal models simulated fasting or average daily glucose and were
106 therefore unable to describe post-prandial responses or responses to glucose challenges such as OGTTs
107 and IVGTTs. A recent model (24) added the capability of following daily and post-challenge glucose
108 variations and was fit to OGTT data from the DPP. It also introduced a distinction between peripheral
109 and hepatic insulin resistance in order to account for the effects of drug and lifestyle interventions on
110 these parameters.
111
112 We also, using a different methodology, introduce simulations of OGTTs at selected points during
113 progression, and separate representations for hepatic and peripheral insulin resistance. We use these new
114 features to differentiate progression by either 2hPG or FPG. We perform IVGTTs as well to illustrate the
115 evolution of the acute insulin response to glucose (AIRg), often used to assess beta-cell function. This
116 requires the model to simulate first and second phase secretion, which we accomplish by incorporating a
117 previously published model for insulin granule exocytosis (17).
118
119 This study focuses on mechanism and insight, rather than assessment. Instead of fitting parameters to
120 particular data sets, we assume parameters and investigate the trajectories of glycemia and insulin
121 secretion that result. We demonstrate that the model captures known features of diabetes pathogenesis
122 data and provides novel insights and interpretations of the data. We conceptualize this as building a
123 factory, not a product. Once the utility of the model is established, we expect that a wide variety of
124 applications to clinical data will become possible.
125
126 **Materials and Methods**
127

We briefly review the previous version of the model (37) and then describe the enhancements introduced here. The enhanced version has been used to study clinical implications of differences in glucose time courses during an OGTT (19), but was not documented in detail. Parameter values and details of functions not given here are in the Appendix (Supplementary Material).

Previous version of the model

The core element, retained in the new version, is a glucose-insulin feedback loop, represented by two differential equations adapted from the Minimal Model of Bergman and Cobelli (8), who built on models going back to the 1960's (2, 11), as modified in (75):

$$\frac{dG}{dt} = MEAL + HGP - (E_{GO} + S_I I)G \quad (1)$$

$$\frac{dI}{dt} = \frac{\beta}{V} ISR - kI \quad (2)$$

The glucose (*G*) equation (Eq. 1) says that *G* increases on a time scale of hours as a result of meal influx and hepatic glucose production (*HGP*) and decreases as a result of uptake, which has both insulin-independent and insulin-dependent components. The factor S_I in the insulin-dependent term is closely related to the well-known sensitivity to insulin reported by the Minimal Model. The insulin (*I*) equation (Eq. 2) says that *I* decreases due to removal, mainly in the liver, with rate constant *k*, and increases due to secretion by beta cells, where β is the beta-cell mass, *ISR* is the insulin secretion rate per unit mass, and *V* is the volume of distribution. In the original version, *ISR* depended only on *G*, through the rate of beta-cell metabolism *M*:

$$ISR = \sigma \frac{(M+\gamma)^{kISR}}{\alpha_{ISR}^{kISR} + (M+\gamma)^{kISR}} \quad (3)$$

where *M* was assumed to be a sigmoidally-increasing function of *G*:

$$M = \frac{G^{kM}}{\alpha_M^{kM} + G^{kM}} \quad (4)$$

151 The parameter γ in Eq. (3) represents the effect of K(ATP) channel density to shift the glucose
152 dependence of secretion (the triggering pathway (39)); when the channel density is low, γ is high, and
153 shifts the dependence to the left, increasing secretion for the same level of M because Ca^{2+} is higher.
154 Experiments in (34) showed that mouse beta cells in vitro adjust the K(ATP) channel density down in
155 response to sustained (overnight) elevated glucose. This has also been observed in vivo in humans (41,
156 42, 44), along with evidence of reduced insulin clearance, k, (19–21). For the most part, we omit this for
157 simplicity, but we consider the implications of reduced clearance towards the end of Results. This can be
158 viewed as the first line of defense through enhanced beta-cell function against insulin resistance over a
159 time scale of days (e.g. holiday overeating).
160 The value of γ depends on glucose, which is taken into account by adding a third differential equation to
161 the system:
162
163 $$\frac{d\gamma}{dt} = \frac{\gamma_\infty(G) - \gamma}{\tau_\gamma} \quad (5)$$
164
165 where γ_∞ is an increasing sigmoidal function of G, and τ_γ is the time constant.

166 Insulin resistance that persists over longer periods (months in humans) despite reduced K(ATP) channel
167 density, is assumed to trigger a further level of compensatory increased beta-cell function via σ, the
168 maximal insulin secretion capacity (Eq. 3). This corresponds to the amplifying effects of metabolism
169 and/or modulators such as GLP-1 and ACh on the efficacy of Ca^{2+} to drive insulin granule exocytosis.
170 This second aspect of beta-cell functional compensation entails a fourth differential equation:

171 $$\frac{d\sigma}{dt} = \frac{\sigma_\infty(ISR, M) - \sigma}{\tau_\sigma} \quad (6)$$

172 We assume that increased *ISR* (workload in the sense of (64)) leads to an increase in σ whereas

173 increased *M* leads to a decrease in σ.

174 The slowest and final form of compensation for insulin resistance is increased beta-cell mass, β, which

175 develops over years in humans. We assume that β is increased by proliferation, *P*, and decreased by

176 apoptosis, *A*. Following the data of (64), we assume that *P* increases when *ISR* increases. We further

177 assume that apoptosis is largely driven by metabolic stress (e.g. through increased production of reactive

178 oxygen species) when glucose is high, so we make *A* an increasing function of *M* :

179 $$\frac{d\beta}{dt} = \frac{(P(ISR) - A(M))\beta}{\tau_\beta} \quad (7)$$

180

181 The parameters defining *P* and *A* are chosen such that modest increases in *G* result in a net increase in β,

182 but large increases in *G* result in a net decrease in β. As in the predecessor model (75), this leads to a

183 shift from compensation (negative feedback) to decompensation (positive feedback). In (37), we showed

184 that this can account for the threshold behavior observed in both rodents and humans, that is, nearly

185 steady *G* followed by a sharp, essentially irreversible increase (50, 73). We proposed this as an

186 explanation for why prevention of T2D is much easier than reversing it once it is established. The same

187 dynamic properties carry over in this study with the model enhanced as described next.

188

189 ***New features in the model***

190 *Modeling glucose flux during daily meals and glucose tolerance tests*

191 In the previous version of the model (37), *G* represented average daily glucose and insulin levels in

192 response to steady glucose input. To address IFG and IGT, we need to be able to dissociate fasting

193 glucose from post-challenge glucose. The first step is to introduce variable glucose influx from meals,

194 represented by the term *MEAL* in Eq. (1). Timing of meals is standardized to 6:00 AM, 12:00 Noon, and
195 6:00 PM. The expression we use is:

196 $$MEAL = meal_{max}\left(\frac{t^{mk}}{\alpha_{meal}+t^{mk}}\right)^{\eta}\exp(-\mu t) \quad (8)$$

197 and Fig. S3 shows the glucose flux (panel A) and the resulting plasma glucose concentrations (panel B).
198 We do not yet account for other nutrients (amino acids, fats). Flux during an OGTT is modeled with a
199 more rapid rise and decay of flux (Eq. (A2) and shown in Fig. S3, C, D). Flux during an IVGTT rises and
200 decays still more rapidly.

201

202 *Modeling hepatic glucose production (HGP)*

203 In order to distinguish peripheral and hepatic insulin resistance and describe how they are related to each
204 other, we need to refine the model description of hepatic glucose production (*HGP* in Eq. 1). In the first
205 version of the model (37), *HGP* was assumed to be constant, which is an acceptable approximation as
206 long as fasting plasma insulin is adequate to compensate completely for any hepatic insulin resistance.
207 To study the failure of compensation, however, we need to make *HGP* a decreasing function of *I*:

208 $$HGP = \frac{hepa_{max}}{\alpha_{HGP} + hepa_{S_I}I} + HGP_{bas} \quad (9)$$

209 This is sufficient to give the typical drop and recovery of *HGP* after a meal (Fig. S4A).

210 Less obvious, but also important, we need to account for the correlation between hepatic and peripheral
211 insulin resistance, which we do by making two of the parameters in Eq. 8, $hepa_{max}$ and α_{HGP}, functions of
212 S_I:

213 $$hepa_{max} = \frac{hepa_{bar}}{hepa_k + S_I} + hepa_{sh} \quad (10)$$

214 $$\alpha_{HGP} = \frac{\alpha_{bar}}{\alpha_k + S_I} + \alpha_{sh} \quad (11)$$

215

216 Both $hepa_{max}$ and α_{HGP} decrease with S_I, as shown in Figs. S4B, C, and the net effect is that *HGP*
217 decreases as S_I increases (Fig. S4D).

218 If this, or something like this, is not done, then severe peripheral resistance combined with strong
219 compensatory insulin secretion can result in fasting hypoglycemia, which is not the typical pattern (see
220 Fig. S5).

221 In more typical cases of progression to pre-diabetes or diabetes, the relative impairment in insulin
222 secretion would mask this effect: the level of glycemia would be reduced but hypoglycemia would not
223 result. We chose the parameters such that HGP remains normal when insulin is elevated unless there is a
224 defect in beta-cell mass or function.

225 Figure S6, E – H shows the response of HGP and glucose disposal to a simulated hyperinsulinemic,
226 euglycemic clamp, with steady-state values in good agreement with experimental data (6).

227 To represent hepatic insulin resistance over and above the component related to peripheral insulin
228 resistance, we decrease the parameter $hepa_{SI}$ in Eq. A4, which increases HGP at any value of *I*.

229 Equations 9 – 11 are phenomenological expressions that achieve the goals of making *HGP* decrease with
230 *I* and increase when insulin resistance is present, but other expressions could also possibly work. We
231 considered making the value of $hepa_{SI}$ depend on *I* as an alternative way to avoid hypoglycemia, but this
232 did not work well. It is also possible that glucagon, which is not in the model, would help to prevent
233 hypoglycemia (see *Limitations of the study* in the Discussion).

234

235 *Modeling insulin granule exocytosis*

236 To study the dynamics of glucose and insulin under glucose challenges such as meals, OGTT, and
237 IVGTT, the model needs to account for the multiple kinetic components of insulin secretion. We adapted
238 an existing model of insulin granule exocytosis (17), which was designed to capture the biphasic pattern
239 of *ISR* in response to a glucose step in vitro or a hyperglycemic clamp in vivo. The first phase is
240 characterized by a sharp peak of *ISR* during the first 10 minutes and the second phase by a steady increase
241 of *ISR* over the next hour. Figure S6 shows a simulated OGTT (panels A, B) and a simulated IVGTT
242 (panels, C, D) compared to experimental data.

243 These phases are mediated by progression of vesicles through a sequence of stages culminating in
244 exocytosis (fusion with the plasma membrane and release of insulin to the circulation; Fig. S2A). A large
245 reserve pool, treated as an inexhaustible reservoir, feeds the docked pool (vesicles at binding sites on the
246 plasma membrane). Once docked, vesicles are primed and enter the readily releasable pool (RRP).
247 Primed vesicles join the immediately releasable pool by becoming closely associated with voltage-
248 dependent Ca^{2+} channels. First-phase secretion depends mainly on the size of the RRP at basal glucose,
249 and second phase secretion is controlled by the rate of mobilization of vesicles to the docked pool.

250
251 The insulin secretion rate *ISR* in the first version (37) of the model (Eq. 3) is in the new version no longer
252 a function of glucose, but is calculated as an output of the exocytosis model (Eqs. A11), *ISR* thus now
253 depends on the history of exposure to *G*, as it should, not just the current value. The exocytosis model
254 requires as input the cytosolic Ca^{2+} concentration, which is modeled as a sigmoidal function of the beta-
255 cell metabolic rate *M* (Eq. A7), and the much higher Ca^{2+} concentration in the microdomains of Ca^{2+}
256 channels, which is modeled as a function of cytosolic Ca^{2+} (Eq. A8). The dose response curve shift γ,
257 previously included in Eq. 3, represents the dynamic changes in K(ATP) channel density as before, but
258 now explicitly alters cytosolic Ca^{2+} at a given level of *M* (Eq. A7). Cytosolic calcium enhances the rates
259 of mobilization of the reserve pool to the plasma membrane (Eq. A10) and priming of docked vesicles (r_2
260 in Eqs. A12), whereas vesicle fusion is primarily controlled by microdomain Ca^{2+}. The amplifying effect

of glucose (39) is incorporated as a multiplicative factor in the rate of vesicle mobilization (G_F in Eq. A9). The effect of the incretin GLP-1and drugs that mimic it to increase insulin secretion is modeled as enhancing the amplifying effect of glucose by increasing the parameter G_{Fmax} in Eq. A9 and as enhancing vesicle priming by increasing the parameter r_2^0 in Eq. A12. This is in accord with a key feature of these agonists, that they have little or no effect on secretion in the absence of glucose, minimizing the risk of hypoglycemia that plagues sulfonylureas. Fig. S2C shows the effect of a two-fold increase in the incretin effect on insulin secretion rate during a hyperglycemic clamp, in agreement with the effect of the GLP-1 receptor agonist liraglutide in the RISE study (68). Modeling the effect of incretins on glucose is more difficult, as it would require including their effects to inhibit glucagon secretion or promote weight loss, which is not feasible in the current model.

For IVGTT and hyperglycemic clamp simulations, we reduce G_F by about a factor of two to represent the lack of the incretin effect on vesicle mobilization and reduce r_2^0 (Eq. A12) about 10-fold to represent the lack of incretin effect on vesicle priming. The rate of mobilization (Eq. A11) is also assumed to be proportional to the variable σ (Eq. 6), which thus controls the magnitude of second-phase insulin secretion. As a consequence, *ISR* implicitly includes σ as a multiplicative factor, as in Eq. (3) of the simpler, first version of the model (37), and the dynamic evolution of the maximal secretory capacity over long time scales (months) is essentially equivalent.

Equations for insulin sensitivity

With one exception we model peripheral insulin sensitivity as an intrinsic property of the target tissues, muscle, liver and adipose, determined implicitly by obesity and genetics. In the model, this makes it an external, time-dependent parameter of the system, and we examine how hyperinsulinemia compensates

283 for insulin resistance. We model insulin sensitivity, S_I, as an exponentially decreasing function of time,

284 following (75):

285 $$\frac{dS_I}{dt} = \frac{(tar_{SI} - S_I)}{\tau_{SI}} \quad (12)$$

286 In Fig. 9, we consider a hypothesis under current discussion in the literature (35, 65, 71, 74), that insulin

287 resistance may be caused by hyperinsulinemia, rather than the other way around. We think it is

288 implausible that this is the sole cause of insulin resistance, and propose instead that the core component of

289 insulin resistance is due to obesity and genetics but modified by the level of insulin I as a result of the

290 negative feedback generated in the insulin signaling cascade (70). We represent the effect, which we term

291 *induced resistance*, as follows:

292 $$S_I = S_{I,0}E \quad (13)$$

293 where

294 $$\frac{dS_{I,0}}{dt} = \frac{(tar_{SI} - S_{I,0})}{\tau_{SI}} \quad (14)$$

295 and

296 $$\frac{dE}{dt} = \frac{(E_\infty(I) - E)}{\tau_E} \quad (15)$$

297 Equation (15) says that E relaxes towards E_∞ with a time constant τ_E, where E_∞ is a sigmoidally

298 decreasing function of I,

299 $$E_\infty(I) = \bar{E}\left[I - \frac{(I - I_{sh})^{kE}}{\alpha_E{}^{kE} + (I - I_{sh})^{kE}}\right] + E_b, \quad (16)$$

300 several examples of which are shown in Fig. 9F. The time constant τ_E is set to two days so that E, and

301 hence S_I, will respond to sustained hyperinsulinemia, not to normal insulin fluctuations following meals

or glucose tolerance tests. The effect is propagated into hepatic insulin resistance through the terms containing S_I. Other parameters are in the legend for Fig. 9 and Table S17.

Criteria of pre-diabetes and diabetes

Following ADA criteria, we define IFG as FPG > 100 mg/dl but < 126 mg/dl, IGT as 2hPG > 140 mg/dl but < 200 mg/dl, and T2D as FPG ≥ 126 mg/dl or 2hPG ≥ 200 mg/dl. Combined glucose impairment (CGI) is defined as co-occurrence of IFG and IGT.

Software

The model equations are solved using xppaut (5) and Matlab (The Mathworks, Natick, MA). Input files defining the parameters and initial conditions are available on Figshare at: https://doi.org/10.6084/m9.figshare.10792412).

Results

In Figs. 1 – 4, we carry out longitudinal simulations over a period of five years starting in the NGT state in which either peripheral insulin resistance is dominant, in which case the first stage of hyperglycemia is IGT, or hepatic insulin resistance is dominant, in which case the first stage of hyperglycemia is IFG. These assumptions are applied by modeling peripheral and hepatic insulin sensitivity as exponentially decreasing, using Eqs. A13 and A14, respectively. The initial values and rates of decline are the same for all figures, but the steady state (target) values, tar_{SI} and tar_{hepaSI}, are varied. The simulations calculate the daily responses to meals, but we plot only the results of OGTTs carried out periodically over the five-year

324 time span by pausing the longitudinal simulation. The corresponding peak postprandial glucose is shown
325 in Fig. S7. The capacity of beta-cell function to compensate for insulin resistance is assumed to be
326 limited, except in Fig. 2. The defect consists of a right shift in γ_∞ relative to Fig. 2, which can be
327 interpreted as a slight gain of function mutation in KCNJ11, the Kir6.2 component of the KATP channels.
328 Alterations in σ_∞ representing a mild defect in insulin granule mobilization would have a similar effect.

329 Parameters that were varied to make the figures are listed in Table S12A in the Appendix, and the initial
330 conditions for Figs. 1 – 4 are in Table S12B.

331

332 ***IGT-first pathway***

333 Figure 1 shows a longitudinal simulation of the effects of a strong decrease in peripheral insulin
334 sensitivity S_I (Fig. 1A) combined with a mild decrease in hepatic insulin sensitivity, $hepa_{SI}$ (Fig. 1B). As
335 insulin resistance progresses, 2hPG increases rapidly while FPG increases more slowly (Fig. 1C),
336 resulting in progression from normal glucose tolerance (NGT) to IGT, CGI and ultimately T2D (Fig. 1C).

337 Fasting plasma insulin (FPI) and 2-hour plasma insulin (2hPI) rise as the beta cells initially compensate
338 partially for the insulin resistance, then fall as the beta cells fail (Fig. 1D), following the classic "Starling
339 law" of the pancreas (27). The initial rise in secretion results from an increase in beta-cell sensitivity to
340 glucose (the variable γ increases, not shown), and the decline results from a fall in the slower component
341 of beta-cell function, σ (Fig. 1E). Beta-cell mass (β) also rises and falls, but the variation is limited
342 because of the slowness of β, and the fall occurs only after T2D is already underway (Fig. 1F). This
343 accords with observations that beta-cell mass is elevated in insulin-resistant pre-diabetics but reduced in
344 long-standing diabetes (15, 66, 69).

345 A subtle but important point of this simulation is that insulin resistance in both the liver and peripheral
346 tissues reaches saturation (Fig. 1A, B) well before the advent of T2D. It is rather the continuing fall in
347 beta-cell function, σ, that drives conversion to T2D. The same sequence was seen in the simulation of
348 T2D progression in Zucker diabetic fatty rats (Fig. 6 in (37)) and in data from monkeys (10).

349 The fall in σ is triggered by the hyperglycemia and glucotoxicity that follows the early loss of insulin
350 sensitivity (Fig. 1D) but would not lead to T2D if the pre-existing capacity of beta-cell function to
351 compensate were stronger. This is illustrated by a simulation with the same degree of insulin resistance
352 as in Fig. 1, but a milder beta-cell defect, which mimics a non-diabetic subject with insulin resistance
353 (Fig. 2). FPG and 2hPG increase modestly in response to insulin resistance and reach a plateau in the
354 IGT state as σ levels off (Fig. 2E) and plasma insulin plateaus (Fig. 2D). The limitation of the rise in
355 glucose reduces the effects of glucotoxicity and buys time for beta-cell mass to increase and stabilize the
356 IGT state (Fig. 2F).

357 Figures 1 and 2 together paint a picture in which not only is a combination of insulin resistance and
358 impaired secretion necessary for T2D, but insulin resistance develops and saturates first, and T2D
359 develops only if the beta cells fail. Some defect in beta-cell function is required even for pre-diabetes, in
360 agreement with (28). Conversely, a pre-existing defect in insulin secretion would be silent in the absence
361 of insulin resistance (Fig. S8), unless it were severe (Fig. S9).

362

363 ***IFG-first pathway***

364 In Fig. 3 we illustrate a contrasting case to Fig. 1, dominant hepatic insulin resistance with minor
365 peripheral resistance (Fig. 3A, B); the same beta-cell function defect is assumed as in Fig. 1. Hepatic
366 insulin resistance drives FPG across the threshold for IFG, while 2hPG remains below the threshold for
367 IGT (Fig. 3C). After the initial threshold crossing, however, FPG and 2hPG continue to rise, and IFG

368 progresses to CGI as in Fig. 1. Insulin again rises with the help of γ (not shown) and falls when the drop
369 in σ becomes too great (Fig. 3E). As in the IGT-first pathway, the conversion to T2D is driven mainly
370 by reduced beta-cell function, σ, because insulin resistance in both the liver and peripheral tissues
371 saturates well before T2D (or even CGI) begins. Beta-cell mass again plays a minor role (Fig. 3F).

372 In the BLSA some subjects who had progressed from NGT to IGT went on to T2D at the next follow-up,
373 which prompted the authors to ask whether CGI could be skipped (51). Figure 4 demonstrates that this
374 can happen if peripheral insulin resistance is made much greater than hepatic resistance (compare Fig. 4A
375 to Fig. 1A). Extreme loss of peripheral insulin sensitivity causes 2hPG to rise dramatically, while FPG
376 remains in the normal range, converting NGT to IGT. 2hPG continues to deteriorate without a substantial
377 increase in FPG, resulting in progression of IGT to T2D without passing through CGI. Eventually, FPG
378 crosses the thresholds for IFG and T2D, but after the individual has already reached T2D based on 2hPG.

379 Figures 1 and 3, respectively, consider extreme cases of peripheral insulin resistance (PIR), where S_I
380 dominates, and hepatic insulin resistance (HIR), where $hepa_{SI}$ dominates . However, most people on the
381 path to T2D will have both. A composite view of the cases of Figs. 1 and 3 together with intermediate
382 phenotypes is given in Fig. 5, where trajectories are plotted in the FPG – 2hPG plane. The only
383 difference among the trajectories is the degree of HIR and PIR, varied inversely from lower right to upper
384 left; the compensatory capacity of beta-cell function is identical for all traces. Fig. 5A shows that the
385 trajectories diverge markedly as the defects in HIR and PIR set in but converge as hyperglycemia
386 worsens; this happens because IFG induces IGT and IGT induces IFG. Thus, all the virtual patients end
387 up looking the same as time goes on. The latter part of the NGT stage and the early part of the IGT stage,
388 shown expanded in Fig. 5B, are when the underlying pathologies give rise to the most distinct behavior.
389 This is important both for designing clinical studies and for stratifying patients for treatment. The figure
390 suggests that the slope of the trajectory from two or more OGTTs spaced suitably far apart in time could
391 give a good indication of the future path of the patient.

392 We next look more closely at the pathogenesis process as it would appear clinically by simulating OGTTs
393 (Fig. 6) and IVGTTs (Fig. 7) at representative times for each stage of glucose tolerance, indicated by the
394 black circles on the time axes in Figs. 1C and 3C.

395

396 ***Simulation of OGTTs***

397 Figure 6A, C shows representative glucose and insulin profiles during OGTTs at each stage of the IGT-
398 first pathway of Fig. 1. Insulin concentrations at the IGT stage (Fig. 6C, dotted curve) are increased
399 compared to NGT (Fig. 6C, solid curve) but are inadequate to maintain normoglycemia at two-hours
400 because of the decreased peripheral insulin sensitivity (Fig. 1A). In contrast, the level of fasting insulin at
401 IGT (Fig. 6C, dotted curve) is sufficient to maintain fasting glucose within the normal range because
402 hepatic insulin resistance is relatively mild (Fig. 1B). During CGI, glucose (Fig. 6A, dashed curve) is
403 increased at all time points compared to IGT, while the insulin level (Fig. 6C, dashed curve) is slightly
404 diminished at the early time points (relative to glucose, however, secretion is impaired at all time points).
405 This indicates that even progression to CGI from IGT is mainly due to impaired beta-cell function.
406 Further and more marked decreases in insulin, due to impaired secretion at all time points during the
407 OGTT, lead to diabetes (dot-dashed curve). Thus, during the progression towards T2D, insulin at all time
408 points during the OGTT first increases and then decreases, in accord with the Starling Law (27).

409 Figure 6B, D shows glucose and insulin at each stage of the IFG-first pathway of Fig. 3. Severe hepatic
410 insulin resistance increases glucose at all time points during the OGTT (Fig. 6B). The increase in FPG is
411 greater than for 2hPG, so the threshold for IFG is crossed first in Fig. 3. Even though fasting insulin at
412 the IFG stage (Fig. 6D, dotted curve) is very high, it is not enough to maintain normal FPG, because of
413 the severe hepatic insulin resistance (Fig. 3B). However, 2hPG is maintained in the normal range because
414 peripheral insulin resistance is mild (Fig. 3A). Since both peripheral and hepatic insulin sensitivity

415 saturate before the onset of CGI (Fig. 3A, B), the decrease in insulin at all time points during the OGTT
416 (Fig. 6D, dashed curve) due to falling beta-cell function (Fig. 3E) is the main contributor to the
417 progression to CGI from IFG and then to T2D.

418

419 ***Simulation of IVGTTs***

420 Figures 1 – 6 highlight the importance of secretion defects, in the context of insulin resistance, in all the
421 pathways to T2D, but now we break out the contributions of early vs. late secretion. First-phase secretion
422 is widely considered a key early marker of future progress. For example, the classic paper (13) reported a
423 cross-sectional study of IVGTTs, and showed that AIRg declines as FPG rises and is nearly gone by the
424 time FPG reaches 115 mg/dl, well below the threshold for T2D. This supports the use of AIRg, and by
425 implication first-phase insulin secretion, as an early marker for T2D. We now show that the model can
426 reproduce the negative correlation between FPG and AIRg, but that rising FPG is not necessarily the sole
427 or proximal cause of the decline in AIRg.

428 Figures 7A, B show simulations of the insulin responses during IVGTTs performed during the IGT-first
429 and IFG-first pathways, respectively. AIRg is blunted and then vanishes in both pathways as FPG rises,
430 as found in (13), but 2hPG also rises at the same time, albeit to different degrees relative to FPG in the
431 two pathways. The decline of AIRg is more rapid than seen experimentally along both pathways (14), but
432 the main point is that it results from the decline of RRP size (Figs. 7C, D), which is more fundamental
433 than the level of glycemia, as the next two paragraphs explain.

434 RRP size is controlled by two factors, the rate of secretion, which determines the rate of vesicle efflux
435 from the RRP and the rate of vesicle influx into the RRP from the docked pool. High FPG increases the
436 rate of efflux in the basal state, so the RRP will already be depleted when the IVGTT commences, and
437 AIRg will consequently be reduced. The rate of influx depends on the size of the docked pool and the

438 rate of priming of docked vesicles. The rate of priming does not vary much in our simulations, but the
439 size of the docked pool does, depending mainly on the rate of docking, which is proportional to one of our
440 beta-cell function variables, σ. Although modest increases in glucose stimulate vesicle docking, larger
441 increases cause glucose toxicity, which reduces σ and hence docking.

442 Because σ is slow, it responds to the average daily glucose, including the contributions of both fasting
443 and post-prandial glucose, which differ according to pathway. Along the IGT-first pathway (Figs. 1 and
444 7A, C), AIRg initially declines primarily because of reduced σ (Fig. 1E), which is mainly determined by
445 high post-prandial glucose, rather than FPG. Positive feedback in turn drives post-prandial glucose
446 higher as σ decreases (Figs. 1C, E). Thus, the loss of AIRg and first-phase secretion is an indirect
447 consequence of diminished second-phase secretion capacity. As the subject progresses to CGI, FPG also
448 rises and further reduces AIRg due to pool depletion. In contrast, during the IFG-first pathway (Figs. 3
449 and 7B, D), the early rise of FPG reduces AIRg by depleting the RRP, and positive feedback from the
450 later rise of 2hPG further diminishes AIRg by driving down σ.

451 In summary, reduced AIRg can be a marker of impairment in either first- or second-phase secretion, and,
452 as glycemia progresses towards T2D, is likely to indicate both.

453

454 ***Targeted Drug Therapy***

455 With the previous, simpler model (37) we showed that NGT and T2D were bistable states separated by a
456 threshold. This accounted for the well-known observation that it is easier to prevent T2D than to reverse
457 it. The new model retains these characteristics but raises the possibility that the response to therapeutic
458 interventions may vary depending on which pathway a patient follows to T2D. Figure 8 shows that this is
459 indeed the case, and that knowledge of a patient's subtype of insulin resistance can in principle lead to
460 more effective drug therapy.

461 Figures 8A, B contrast two drug therapies targeted to peripheral vs. hepatic insulin resistance in patients
462 in the early stages of diabetes. Figure 8A shows glucose for a patient on the IGT-first pathway with
463 dominant peripheral insulin resistance as in Fig. 1, in the absence of therapy (control, black curves) or in
464 response to a high dose of a drug targeted to peripheral insulin resistance (dashed curves) or a drug
465 targeted to hepatic insulin resistance (dotted). The high dose of the appropriately targeted drug only
466 transiently improves FPG and 2hPG and ultimately fails to reverse T2D. Nonetheless, it is more effective
467 at delaying progression than the mistargeted drug.

468 Figure 8B represents the complementary case, a patient on the IFG-first pathway with dominant hepatic
469 insulin resistance, as in Fig. 3. The same treatments are applied, and, as in panel A, both drugs only
470 transiently improve FPG and 2hPG, but the appropriately targeted drug is more effective at delaying
471 progression.

472 Figures 8C, D show the same drug therapies and progression pathways as in panels A and B, but with the
473 drugs applied before the onset of diabetes. A low dose of a drug targeted to the patient's specific insulin
474 resistance pathology is in both cases now able to prevent progression to diabetes, while a low dose of a
475 mistargeted drug only delays progression. These examples suggest that the effectiveness of drug therapy
476 depends on both early initiation of treatment and detection of the major metabolic abnormality.

477 The study in (24) found that it was necessary to assume that the efficacy of treatment wanes with time in
478 order to fit the data from lifestyle and drug interventions in the DPP. Here we have shown that even if the
479 efficacy of treatment is maintained, the intrinsic dynamics of progressive beta-cell dysfunction can cause
480 treatment to fail.

481 Caution should be used in interpreting the simulated treatments in Fig. 8 in terms of currently used drugs.
482 For example, in the DREAM study (29) it was found that rosiglitazone was effective in cases of isolated
483 IFG (IIFG), that is IFG in the absence of IGT. Although rosiglitazone is often thought of as primarily

484 improving peripheral insulin sensitivity, it also improves hepatic insulin sensitivity (81). In addition,
485 IIFG does not necessarily imply pure hepatic insulin resistance. For example, a person with FPG = 115
486 and 2hPG = 135 would be classified as IIFG but may have significant peripheral insulin resistance. Most
487 individuals with pre-diabetes likely have a mixture of peripheral and hepatic insulin resistance.

488 ***Hepatic Insulin Clearance***

489 Another way to generate a compensatory increase in insulin is to reduce clearance. There is considerable
490 evidence that insulin clearance is positively correlated with peripheral insulin sensitivity (3, 63), but the
491 direction of causation is not clear. If clearance is reduced secondary to reduced overall insulin sensitivity,
492 then the increased insulin would contribute to the compensatory response, along with increased secretion.
493 However, it has been suggested that the increased insulin resulting from reduced clearance may also
494 contribute to insulin resistance (61). In Fig. 9, we explore the consequences of reduced clearance,
495 assuming that the increased insulin reduces S_I is reduced by varying degrees as I is increased, as described
496 in Methods. We assume for simplicity that clearance itself is constant throughout each simulation rather
497 than adapting to glucose, insulin or insulin sensitivity. The control case, shown in black, is equivalent to
498 Fig. 1, an example of an IGT-first pathway to T2D. If clearance is reduced, and a modest degree of
499 additional insulin resistance is assumed (green curve in panel F), such that the S_I is only slightly lower
500 than the control case (panel A), then the progression to T2D is delayed (compare black and green curves
501 in panel C). (The smallness of the difference in S_I is due to the fact that glucose is elevated to levels
502 where the induced effect is triggered only for a brief period of each day.) Note that σ is slightly larger
503 (green vs. black, panel E), indicating that reducing clearance partially spared beta-cell function.

504 If the effect of insulin to induce resistance is made larger (blue curves), the beneficial effect of higher I
505 due to reduced clearance and the harmful effect of reduced insulin sensitivity approximately cancel out.
506 Finally, if the induced resistance effect is made extreme, such that even a slight increase in I reduces S_I in
507 half (red curves), the net effect is somewhat accelerated progression. We conclude that induced insulin

508 resistance makes at best a modest contribution to the progression to T2D. If an even more extreme
509 degree of induced resistance is assumed, such that even a slight increase in I reduces S_I to near 0, then it is
510 possible for frictional resistance to be the main driver of T2D, but we consider such a scenario
511 implausible.

512

513 ***Non-Insulin-Mediated Glucose Uptake***

514 We have focused up to this point on the contributions of hepatic and peripheral insulin resistance in
515 driving the IFG-first and IGT-first pathways. However, non-insulin-mediated glucose uptake, also known
516 as glucose effectiveness, is comparable in magnitude to insulin-dependent uptake (9) and has been found
517 to be impaired in T2D (30). It is thus a potential target of drug therapy. We model this by varying the
518 model parameter E_{G0} (similar to S_g in Minimal Model analysis) in Eq. 1. In Fig. S10 we demonstrate that
519 cutting glucose effectiveness in half can result in T2D in someone otherwise not at risk, such as the case
520 shown in Fig. 2. Conversely, in Fig. S11 we show that doubling glucose effectiveness can prevent T2D
521 in someone otherwise predisposed, such as the case shown in Fig. 1.

522

523 **Discussion**

524 In recognition of the fundamental character of type 2 diabetes (T2D) as a progressive disease that
525 develops over many years, we have established a longitudinal model for its pathogenesis. We follow in
526 the footsteps of other longitudinal models (23, 24, 75) but offer new clinical applications and insights.

527 We apply the model to analyze the diverse presentation of hyperglycemia, which may manifest first in
528 fasting glucose (IFG-first pathway) or two-hour glucose during an OGTT (IGT-first pathway). To carry
529 out this program, we modified the representation for beta-cell response to insulin resistance in the first

530 version of the model (37), enhancing it to differentiate between hepatic and peripheral insulin resistance.
531 The simulations show that heterogeneity in the degree of the two forms of insulin resistance can account
532 for a wide variety of observed patterns, supporting the idea of T2D as a unitary disease with quantitative
533 variants. We have focused on extreme cases to highlight the differences (e.g. Fig. 1 vs. Fig. 3), but the
534 family of trajectories in the FPG-2hPG plane (Fig. 5) shows that these lie on a continuum. Figure 5 also
535 highlights that differences in insulin resistance phenotype are most evident in the late NGT and early pre-
536 diabetes stages, which are thus most amenable to differential phenotyping and therapeutic stratification.

537 We have incorporated a description of insulin granule dynamics sufficient to account for both first- and
538 second-phase insulin secretion. This made it possible to simulate OGTT and IVGTT time courses and
539 show how they are transformed systematically during progression along the two canonical pathways to
540 diabetes (Figs. 6, 7). We also showed that sufficiently strong beta-cell function can prevent T2D even
541 when insulin resistance is severe, allowing individuals to maintain a permanent state of IGT (Fig. 2) or
542 even revert from IGT to NGT (not shown). Conversely, sufficient insulin sensitivity can prevent T2D
543 even when beta-cell function is somewhat impaired (37). As discussed below under *Secretion defects*, a
544 fuller treatment of the differences in the balance of insulin secretion and insulin action defects is needed
545 to account fully for the diverse patterns of T2D progression.

546 We summarize below the specific lessons learned and questions answered by this study and give a
547 preview of the clinical applications we anticipate for the model.

548

549 ***Questions raised in the BLSA and other studies***

550

551 The BLSA study (51) asked whether subjects who enter the IGT state necessarily pass through CGI on the
552 way to T2D. The model suggests (Fig. 4) that this is not the case, but skipping CGI happens only if the
553 peripheral insulin resistance is markedly greater than hepatic insulin resistance, which may be relevant for
554 adolescents, who experience extreme obesity and insulin resistance. An intermediate possibility predicted

555 by the model is a short, but not absent, interval of CGI that could escape detection if the follow-up
556 interval is too long.

557 A parallel question is whether individuals can go directly from IFG to T2D without passing through CGI.
558 This is harder than going directly from IGT to T2D because 2hPG is much more labile than FPG; it is
559 difficult to get an increase in FPG sufficient to cross the threshold for T2D (125 mg/dl) without at the
560 same time having 2hPG cross the threshold for IGT (140 mg/dl). Indeed, we have not been able to
561 simulate this scenario just by choosing an appropriate mixture of hepatic and peripheral insulin sensitivity
562 using the other parameters as in Figs. 1 – 4, but model simulations (not shown) predict that it can happen
563 if a more severe beta-cell defect (in γ_∞, Eq. A15) is assumed.

564 The BLSA study also asked whether individuals can pass directly from NGT to T2D without passing
565 through any pre-diabetic state. Because glucose is in quasi-steady state with the much slower variables
566 representing beta-cell mass, beta-cell function and insulin sensitivity, this is not possible in the model
567 unless one of those slow variables undergoes a catastrophic, virtually discontinuous, change.
568 Pancreatectomy would be an example of this, but even type 1 diabetes, triggered by a rapid fall in beta-
569 cell mass, has a distinct prediabetes phase. The cases observed in the BLSA in which subjects were NGT
570 at baseline and T2D at first follow-up most likely reflected rapid progression or a long gap between visits.
571 Similarly, the model simulations indicate that it is unlikely for individuals to go from NGT to CGI
572 without passing through IFG or IGT.

573 The BLSA reported that IFG is generally followed by IGT and IGT is generally followed by IFG, and the
574 model suggests that each state *induces* the other. This happens because the initial rise in glucose during
575 IFG impairs beta-cell function, which causes 2hPG to rise, and vice versa. Another study raised the
576 question of whether CGI is a progressed state of IFG (57); the model simulations together with the BLSA
577 data show that CGI may instead be a progressed state of IGT, to which IFG has been added.

578 One can also ask whether crossing the threshold for FPG or 2hPG of pre-diabetes predicts whether T2D
579 will be reached by crossing the corresponding threshold. In Fig. 1, IGT is followed by T2D diagnosed
580 through 2hPG, and further simulations with the model (Fig. 5) suggest that this is typical. In Fig. 3, IFG
581 is followed by T2D diagnosed through FPG, but further simulations (not shown) indicate that this may or
582 may not be the case, depending on the degree of discrepancy between HIR and PIR and the strength of γ
583 to control FPG.

584 Both the IFG- and IGT-first pathways exhibit elevated fasting insulin. This may account for the
585 observation that elevated fasting insulin was a better predictor of future diabetes in a prospective study
586 than fasting glucose, which is elevated early on only in the IFG-first pathway (22); it may not be
587 necessary to hypothesize a major causative role for high fasting insulin itself. Indeed, in the IGT-first
588 pathway, which is more common, fasting glucose may be suppressed by the compensatory increase in
589 beta-cell function (our variable σ) induced by high post-load glucose (compare Figs. 1 and 4 to Fig. 3).

590 The suppression of fasting glucose in the context of a predominance of peripheral insulin resistance has
591 particular importance for pre-diabetes screening in populations that are prone to IGT but not IFG. This
592 applies notably to people of African descent, for whom fasting glucose has markedly reduced sensitivity
593 for detecting pre-diabetes and diabetes (77). The problem is exacerbated for Africans living in Africa,
594 where measuring 2hPG with OGTTs is prohibitively expensive. The model suggests that in this and
595 similar cases, lowering the threshold for diagnosing pre-diabetes based on fasting glucose could be a cost-
596 effective strategy. More generally, the model points to the need for population- and patient-specific
597 thresholds for diagnosis, which may contribute to resolving current debate on whether prediabetes is a
598 useful diagnosis (62).

599

600 ***Insulin action defects***

601 We have varied peripheral and hepatic insulin resistance independently to study their contributions to
602 T2D progression, but in reality, they are related. Statistically, they are correlated with a coefficient of
603 about 0.7 (1). This is expected for several reasons. For one, they share major components of the insulin
604 signaling pathway. Also, there is evidence that an important determinant of hepatic insulin resistance is
605 excess supply of free fatty acid (FFA) substrate from adipose tissue (58). Thus, insulin resistance in
606 adipose cells would increase lipolysis and FFA flux to the liver, which would drive increased
607 gluconeogenesis (59). On the other hand, the liver has unique roles in glucose and lipid production not
608 shared with muscle, which may account for the fact that the correlation is imperfect.

609 To address hepatic insulin resistance above and beyond the component correlated with peripheral insulin
610 resistance, we have independently varied the affinity of HGP for insulin (parameter $hepa_{SI}$ in Eq. 9), the
611 effect of which is shown in Fig. S4. We have obtained similar results (not shown) by varying the
612 maximal rate of HGP (parameter $hepa_{max}$).

613 Although we have primarily treated insulin resistance as an external influence on the model, representing
614 genetic and obesity, we have considered the much discussed hypothesis (65, 71, 74) that hyperinsulinemia
615 can contribute to insulin resistance in addition to being a compensatory response to insulin resistance
616 (Fig. 9). Any effect of increased insulin to induce insulin resistance has to be weighed against the effect
617 to enhance glucose uptake, and the outcome would depend on the net effect on the term $S_I I$ in Eq. 1. We
618 find that incorporating induced insulin resistance can either advance or delay the rate of progression to
619 T2D modestly depending on the strength of the two effects. We have not found support for the
620 hypothesis that it is the sole or primary initiating factor: to trigger T2D in the absence of intrinsic,
621 insulin-independent insulin resistance, we had to assume that the insulin-induced resistance is implausibly
622 strong. Similar results would apply if hyperinsulinemia resulted from increased secretion rather than
623 reduced clearance, but one would also have to consider whether in this case the increased beta-cell
624 workload might have an additional deleterious effect.

625

626 We are aware of only one other modeling study (35) that has addressed the role of hyperinsulinemia as a
627 driver of diabetes pathogenesis. More specifically, that thoughtful analysis considered a variant of the
628 model of Topp et al (75) in which *hypersecretion* would reduce S_I. Under that assumption, and an
629 additional assumption that high insulin would impair beta-cell mass, hypersecretion was found to be able
630 to drive progression to T2D. However, increased insulin itself that has been shown to induce insulin
631 resistance (71), so we prefer to have insulin act directly on S_I. As we have said above, the effect of
632 hyperinsulinemia governed by that mechanism is modest.

633 The effects of induced insulin resistance are limited fundamentally because insulin both promotes glucose
634 uptake and contributes to resistance to that uptake. This is analogous to friction in mechanics. The
635 higher the insulin concentration, the more resistance is generated through increased negative feedback in
636 the insulin signaling cascade. Similarly, the faster a car goes, the more wind and rolling resistance it
637 generates. This resistance is not the motive force driving the car forward but a by-product of forward
638 motion that limits its speed. However, resistance is generally not strong enough to prevent acceleration, it
639 just requires more gas to achieve the desired speed. Similarly, the insulin resistance induced by insulin
640 can in most cases be overcome by secreting more insulin.

641

642 ***Insulin secretion defects***

643 The simulations of progression to T2D (Figs. 1, 3, and 4) require some degree of secretion defect in
644 addition to the various combinations of insulin resistance. We assumed a defect only in the triggering
645 pathway (γ), but we have obtained similar results by assuming defects in the amplifying pathway (σ).
646 The assumed triggering defect represents a right shift in the glucose dose response curve, which

647 correspond to a mild gain of function (GOF) mutation of the K(ATP) channels, a prominent GWAS hit
648 (55).

649 Assuming a more significant GOF mutation defect in the model leads to T2D with a lesser degree of
650 insulin resistance (Fig. S8). This is in line with the finding that K(ATP) defects are generally mild (for
651 example, the E23K mutation in the Kir6.2 component of K(ATP), KCNJ11, has an odds ratio of only 1.18
652 (33)), but they are fairly common and therefore may make significant contributions on the population
653 level in combination with insulin action defects.

654 If the K(ATP) defect is sufficiently severe, no insulin resistance is needed at all (Fig. S9). This is the
655 case in neonatal diabetes mellitus (NDM) (4, 47), which is of particular interest because it can be treated
656 effectively with sulfonylureas. This differs from typical T2D in adults, possibly because the drug brings
657 the genetically insufficiently active beta cells to a normal level of activity instead of overdriving them.

658 The examples of Figs. 2, 1, S8 and S9, in that order, lie on a continuum of progressively greater K(ATP)
659 channel function and lesser insulin resistance. As we showed previously in Fig. 5 of Ref. #6, the greater
660 the degree of beta-cell dysfunction, the lesser the degree of insulin resistance required for T2D. In
661 addition to the degree of insulin resistance, the rate of decline of insulin sensitivity is important. Fig. S12
662 shows cases in which a slow decline is compensated whereas a fast decline is not, as shown previously in
663 (75). We emphasize that the requirement for insulin resistance for typical T2D progression is not in
664 contradiction with genome wide studies showing a predominance of beta-cell genes: most people who are
665 overweight or obese become insulin resistant, but only those with beta-cell defects become diabetic. Lean
666 individuals who are not insulin resistant can also develop diabetes, but only if they have severe and rare
667 secretion defects.

668 Although we have focused on the role of insulin resistance in promoting IFG, secretion defects can also
669 lead to IFG with little contribution of insulin resistance. Fig. S13 shows a case with a mild GOF mutation

670 in K(ATP) channels, and Fig. S14 shows a case with a small readily releasable pool due to reduced
671 vesicle priming rate. With more extreme secretion defects, no insulin resistance is needed at all (not
672 shown). These patterns may be of particular relevance to Asian and possibly African populations where
673 secretion defects play a bigger role than insulin resistance in diabetes compared to those of European
674 descent.

675 Another secretory defect that may contribute to diabetes risk is impaired incretin signaling. Figure S15
676 illustrates that such an impairment would accelerate progression in a person predisposed to T2D.

677 The model shows that defects in first- and second-phase secretion are not independent. Impairment in one
678 leads to impairment in the other because of the harmful effects of elevated glucose. The model accounts
679 for classic data (13) showing that the acute insulin response to glucose (AIRg), a surrogate for first phase
680 secretion, declines with even modest increases in FPG during the NGT and pre-diabetic stages. The
681 model shows, however, that second-phase insulin secretion declines in parallel, belying a privileged role
682 for first-phase secretion, as also shown in another modeling study (36). In our model, reduced AIRg
683 results mainly from reduced size of the RRP, which can be caused by impairment in either first-phase or
684 second-phase secretion or both. More generally, any unanswered rise in either fasting or post-prandial
685 glucose impairs both first and second phase secretion, and any defect in either first or second phase
686 secretion raises both fasting and post-prandial glucose. This creates a vicious cycle that drives down both
687 first- and second-phase secretion regardless of which defect is primary. Empirical studies that do not
688 select for early isolated IFG or IGT cases do not show a clear prominence of first phase secretion loss
689 (31), in agreement with the model.

690

691 *Non-insulin mediated glucose uptake*

692 We have also considered briefly glucose effectiveness, the ability of glucose to promote its own uptake
693 independent of insulin (Figs. S10, S11). For simplicity, we have assumed the differences in E_{G0} to be pre-
694 existing and constant in time. However, there is evidence that it is a regulated process; it has been
695 reported to be enhanced by FGF19 acting in the brain and may be related to the glucose intolerance
696 resulting from leptin deficiency in ob/ob mice (52). It may also account for the rescue by leptin of
697 glucose tolerance in insulin-deficient rodents treated with streptozotocin (32). Further progress in
698 modeling this process would benefit from identifying the molecular mechanism(s) underlying it, which
699 are currently not well understood.

700

701

702 ***Limitations of the study***

703 The model as presented here is oversimplified in that it only considers glucotoxicity and neglects other
704 factors that are likely to play a role, such as lipotoxicity (48). We are thus unable at present to address the
705 possible role of hyperinsulinemia to promote hepatic fat accumulation (76). If prolonged, this could lead
706 to liver damage and thus to a worsening of insulin resistance that could outlast the induced resistance we
707 have modeled here (Eqs. 9 – 11), which would resolve if normal insulin levels were restored.

708 In addition, we believe that prolonged high secretion rate is probably harmful beyond the negative effect
709 incorporated in the equation for σ, possibly because of ER stress and/or calcium toxicity (53). Those
710 factors were not included here because they were not needed to account for the pathways considered, but
711 they may be necessary to explain other pathways to T2D and will be addressed elsewhere.

712 To capture the full range of patterns, it is necessary to consider as well pre-existing variation in beta-cell
713 function, not the moment-to-moment beta-cell function, which evolves in response to hyperglycemia, but
714 the innate, genetic capacity of beta-cell function to adapt to hyperglycemia. For example, changing the

715 parameters defining σ_∞ (Eqs. 6, A16) has marked effects on the speed of progression in IGT; we
716 neglected this because it doesn't change the likelihood of entering the IGT state much.

717 We have modeled the suppression of hepatic glucose production as a direct effect of insulin on the liver.
718 However, much if not all of the acute effect of insulin is indirect, mediated by suppression of lipolysis in
719 adipose tissue, which reduces the supply of free fatty acid (FFA) to the liver (58). We consider this an
720 acceptable approximation for our purposes, as post-prandial suppression of lipolysis is roughly a mirror
721 image of the post-prandial rise in insulin. In future, if we want to account for FFA dynamics or adipose-
722 tissue insulin resistance, the model would have to be augmented.

723 We have modeled insulin-dependent glucose uptake as linear in insulin, but it is likely to be non-linear
724 (sigmoidal) (12) and has been suggested to exhibit hysteresis (78). We have not found these features to
725 be necessary to explain the data under consideration, but they can be easily added in the future if the need
726 arises.

727 We have neglected the role of excess glucagon secretion, which results from intrinsic defects in alpha
728 cells or from loss of paracrine regulation of alpha cells due to a relative lack of insulin (21, 56). This has
729 long been recognized to exacerbate post-prandial hyperglycemia in diabetes and pre-diabetes and is a
730 target of GLP-1-based insulin secretagogues. Without glucagon in the model, we are not able to simulate
731 fully the efficacy of that class of drugs, only their effect on insulin secretion. Hyperglucagonemia may
732 also contribute to hepatic insulin resistance, as proposed in recent reviews (26, 80) suggesting that
733 glucagon is part of a liver-alpha cell axis that is primarily devoted to regulating amino acid metabolism.
734 A primary form of glucagon resistance at the liver in this cycle could lead to hyperaminoacidemia and
735 hyperglucagonemia. The latter would contribute to excess hepatic glucose production and IFG in
736 addition to or in place of hepatic insulin resistance. This makes glucagon a tempting therapeutic target.
737 Hyperaminoacidemia and alpha-cell hyperplasia have thwarted many efforts, but some work in this
738 direction continues (72).

739 Other recent developments have shown that glucagon amplifies insulin secretion and thus under normal
740 conditions has a net hypoglycemic effect post-prandially (16, 82). Glucagon is thus now seen to be
741 homeostatic in both low and high glucose under normal conditions but can become anti-homeostatic in
742 diabetes or pre-diabetes. The emerging story is complex, and inclusion in the model is deferred to future
743 studies.

744 We have included only a very simple representation of insulin clearance, assuming a first-order
745 dependence on insulin concentration. We have not distinguished portal from peripheral insulin (63) or
746 considered possible regulation by glucose (60) or free fatty acids (7).

747

748 ***Future directions***

749 This paper has demonstrated that if the insulin resistance phenotype of an individual is known, their
750 future trajectory of hyperglycemia can be predicted (Figs. 1 – 4) and drug choice can potentially be
751 optimized for the patient's insulin resistance phenotype (Fig. 8). Another longitudinal model has shown
752 similarly the results of targeting insulin resistance vs. beta-cell replication (38). Our model can provide
753 similar predictions if the relative impairments in insulin secretion and insulin resistance are known. For
754 example, plotting 1hPG vs. 2hPG obtained by simulating OGTTs results in a family of trajectories similar
755 to the ones for FPG vs. 2hPG shown in Fig. 5. The differences in trajectories due to the contributions of
756 insulin secretion and insulin action can be read off from the difference between 1hPG and 2hPG and are
757 similarly most pronounced during prediabetes (Ha et al, ADA poster 1490-P, June, 2019). This
758 prediction may provide deeper insight into the diagnostic information that can be extracted from different
759 time points during the OGTT, an issue that is currently receiving much attention (19, 40).

760 Future versions of the model should include roles for glucagon, as described above. In addition, a more
761 complex model for insulin signaling would permit the investigation of the effects of particular defects in

762 those pathways as well as possible mechanisms for the insulin resistance induced by insulin, which was
763 treated phenomenologically here.

764 In addition, to be a useful tool for patient stratification and treatment planning, one needs to ascertain the
765 patient's phenotype. We plan to investigate whether the model can be used, with suitable modifications,
766 to solve the inverse problem of inferring the individual's parameters of insulin resistance and beta-cell
767 function from the observed behavior.

768

769 **Acknowledgments**

770 The work was supported by the Intramural Research Program of the National Institutes of Health,
771 NIDDK. We thank Stephanie Chung, Richard Bertram, Over Cabrera, and Cecilia Diniz Behn for helpful
772 suggestions on the manuscript.

773

774 # References

775 1. **Abdul-Ghani MA**, **Matsuda M**, **DeFronzo RA**. Strong association between insulin resistance in liver
776 and skeletal muscle in non-diabetic subjects. *Diabet Med* 25: 1289–1294, 2008. doi:
777 10.1111/j.1464-5491.2008.02597.x.

778 2. **Ackerman E**, **Rosevear JW**, **McGuckin WF**. A Mathematical Model of the Glucose-tolerance test.
779 *Phys Med Biol* 9: 203–213, 1964. doi: 10.1088/0031-9155/9/2/307.

780 3. **Ader M**, **Stefanovski D**, **Kim SP**, **Richey JM**, **Ionut V**, **Catalano KJ**, **Hucking K**, **Ellmerer M**, **Van Citters**
781 **G**, **Hsu IR**, **Chiu JD**, **Woolcott OO**, **Harrison LN**, **Zheng D**, **Lottati M**, **Kolka CM**, **Mooradian V**,
782 **Dittmann J**, **Yae S**, **Liu H**, **Castro AVB**, **Kabir M**, **Bergman RN**. Hepatic insulin clearance is the
783 primary determinant of insulin sensitivity in the normal dog. *Obesity (Silver Spring)* 22: 1238–1245,
784 2014. doi: 10.1002/oby.20625.

785 4. **Ashcroft FM**, **Puljung MC**, **Vedovato N**. Neonatal Diabetes and the KATP Channel: From Mutation to
786 Therapy. *Trends Endocrinol Metab* 28: 377–387, 2017. doi: 10.1016/j.tem.2017.02.003.

787 5. **Bard Ermentrout**. Simulating, Analyzing, and Animating Dynamical Systems [Online]. SIAM.
788 http://www.math.pitt.edu/~bard/xpp/xpp.html.

789 6. **Basu R**, **Barosa C**, **Jones J**, **Dube S**, **Carter R**, **Basu A**, **Rizza RA**. Pathogenesis of prediabetes: role of
790 the liver in isolated fasting hyperglycemia and combined fasting and postprandial hyperglycemia. *J*
791 *Clin Endocrinol Metab* 98: E409-417, 2013. doi: 10.1210/jc.2012-3056.

792 7. **Bergman RN**, **Ader M**. Free fatty acids and pathogenesis of type 2 diabetes mellitus. *Trends*
793 *Endocrinol Metab* 11: 351–356, 2000.

794 8. **Bergman RN**, **Ider YZ**, **Bowden CR**, **Cobelli C**. Quantitative estimation of insulin sensitivity. *Am J*
795 *Physiol* 236: E667-677, 1979.

796 9. **Best JD**, **Kahn SE**, **Ader M**, **Watanabe RM**, **Ni TC**, **Bergman RN**. Role of glucose effectiveness in the
797 determination of glucose tolerance. *Diabetes Care* 19: 1018–1030, 1996. doi:
798 10.2337/diacare.19.9.1018.

799 10. **Bodkin NL**, **Metzger BL**, **Hansen BC**. Hepatic glucose production and insulin sensitivity preceding
800 diabetes in monkeys. *Am J Physiol* 256: E676-681, 1989.

801 11. **Bolie VW**. Coefficients of normal blood glucose regulation. *J Appl Physiol* 16: 783–788, 1961. doi:
802 10.1152/jappl.1961.16.5.783.

803 12. **Bonadonna RC**, **Groop L**, **Kraemer N**, **Ferrannini E**, **Del Prato S**, **DeFronzo RA**. Obesity and insulin
804 resistance in humans: a dose-response study. *Metab Clin Exp* 39: 452–459, 1990. doi:
805 10.1016/0026-0495(90)90002-t.

806 13. **Brunzell JD**, **Robertson RP**, **Lerner RL**, **Hazzard WR**, **Ensinck JW**, **Bierman EL**, **Porte D**. Relationships
807 between fasting plasma glucose levels and insulin secretion during intravenous glucose tolerance
808 tests. *J Clin Endocrinol Metab* 42: 222–229, 1976. doi: 10.1210/jcem-42-2-222.

809 14. **Brunzell JD**, **Robertson RP**, **Lerner RL**, **Hazzard WR**, **Ensinck JW**, **Bierman EL**, **Porte D**. Relationships
810 between fasting plasma glucose levels and insulin secretion during intravenous glucose tolerance
811 tests. *J Clin Endocrinol Metab* 42: 222–229, 1976. doi: 10.1210/jcem-42-2-222.

812 15. **Butler AE**, **Janson J**, **Bonner-Weir S**, **Ritzel R**, **Rizza RA**, **Butler PC**. Beta-cell deficit and increased
813 beta-cell apoptosis in humans with type 2 diabetes. *Diabetes* 52: 102–110, 2003. doi:
814 10.2337/diabetes.52.1.102.

815 16. **Capozzi ME**, **Wait JB**, **Koech J**, **Gordon AN**, **Coch RW**, **Svendsen B**, **Finan B**, **D'Alessio DA**, **Campbell**
816 **JE**. Glucagon lowers glycemia when β-cells are active. *JCI Insight* 5, 2019. doi:
817 10.1172/jci.insight.129954.

818 17. **Chen Y**, **Wang S**, **Sherman A**. Identifying the targets of the amplifying pathway for insulin secretion
819 in pancreatic beta-cells by kinetic modeling of granule exocytosis. *Biophys J* 95: 2226–2241, 2008.
820 doi: 10.1529/biophysj.107.124990.

821 18. **Choy S**, **Kjellsson MC**, **Karlsson MO**, **de Winter W**. Weight-HbA1c-insulin-glucose model for
822 describing disease progression of type 2 diabetes. *CPT Pharmacometrics Syst Pharmacol* 5: 11–19,
823 2016. doi: 10.1002/psp4.12051.

824 19. **Chung ST**, **Ha J**, **Onuzuruike AU**, **Kasturi K**, **Galvan-De La Cruz M**, **Bingham BA**, **Baker RL**,
825 **Utumatwishima JN**, **Mabundo LS**, **Ricks M**, **Sherman AS**, **Sumner AE**. Time to glucose peak during
826 an oral glucose tolerance test identifies prediabetes risk. .

827 20. **Cobelli C**, **Dalla Man C**, **Toffolo G**, **Basu R**, **Vella A**, **Rizza R**. The oral minimal model method.
828 *Diabetes* 63: 1203–1213, 2014. doi: 10.2337/db13-1198.

829 21. **D'Alessio D**. The role of dysregulated glucagon secretion in type 2 diabetes. *Diabetes Obes Metab*
830 13 Suppl 1: 126–132, 2011. doi: 10.1111/j.1463-1326.2011.01449.x.

831 22. **Dankner R**, **Chetrit A**, **Shanik MH**, **Raz I**, **Roth J**. Basal-state hyperinsulinemia in healthy
832 normoglycemic adults is predictive of type 2 diabetes over a 24-year follow-up: a preliminary
833 report. *Diabetes Care* 32: 1464–1466, 2009. doi: 10.2337/dc09-0153.

834 23. **De Gaetano A**, **Hardy T**, **Beck B**, **Abu-Raddad E**, **Palumbo P**, **Bue-Valleskey J**, **Pørksen N**.
835 Mathematical models of diabetes progression. *Am J Physiol Endocrinol Metab* 295: E1462-1479,
836 2008. doi: 10.1152/ajpendo.90444.2008.

837 24. **De Gaetano A**, **Hardy TA**. A novel fast-slow model of diabetes progression: Insights into mechanisms
838 of response to the interventions in the Diabetes Prevention Program. *PLoS ONE* 14: e0222833,
839 2019. doi: 10.1371/journal.pone.0222833.

840 25. **de Winter W**, **DeJongh J**, **Post T**, **Ploeger B**, **Urquhart R**, **Moules I**, **Eckland D**, **Danhof M**. A
841 mechanism-based disease progression model for comparison of long-term effects of pioglitazone,
842 metformin and gliclazide on disease processes underlying Type 2 Diabetes Mellitus. *J
843 Pharmacokinet Pharmacodyn* 33: 313–343, 2006. doi: 10.1007/s10928-006-9008-2.

844 26. **Dean ED**. A Primary Role for α-Cells as Amino Acid Sensors. *Diabetes* 69: 542–549, 2020. doi:
845 10.2337/dbi19-0021.

846 27. **DeFronzo RA**. Lilly lecture 1987. The triumvirate: beta-cell, muscle, liver. A collusion responsible for
847 NIDDM. *Diabetes* 37: 667–687, 1988.

848 28. **DeFronzo RA**, **Tripathy D**. Skeletal Muscle Insulin Resistance Is the Primary Defect in Type 2
849 Diabetes. *Diabetes Care* 32: S157–S163, 2009. doi: 10.2337/dc09-S302.

850 29. **DREAM (Diabetes REduction Assessment with ramipril and rosiglitazone Medication) Trial**
851 **Investigators**, **Gerstein HC**, **Yusuf S**, **Bosch J**, **Pogue J**, **Sheridan P**, **Dinccag N**, **Hanefeld M**,
852 **Hoogwerf B**, **Laakso M**, **Mohan V**, **Shaw J**, **Zinman B**, **Holman RR**. Effect of rosiglitazone on the
853 frequency of diabetes in patients with impaired glucose tolerance or impaired fasting glucose: a
854 randomised controlled trial. *Lancet* 368: 1096–1105, 2006. doi: 10.1016/S0140-6736(06)69420-8.

855 30. **Dube S**, **Errazuriz-Cruzat I**, **Basu A**, **Basu R**. The forgotten role of glucose effectiveness in the
856 regulation of glucose tolerance. *Curr Diab Rep* 15: 605, 2015. doi: 10.1007/s11892-015-0605-6.

857 31. **Gerich JE**. Is reduced first-phase insulin release the earliest detectable abnormality in individuals
858 destined to develop type 2 diabetes? *Diabetes* 51 Suppl 1: S117-121, 2002.

859 32. **German JP**, **Thaler JP**, **Wisse BE**, **Oh-I S**, **Sarruf DA**, **Matsen ME**, **Fischer JD**, **Taborsky GJ**, **Schwartz**
860 **MW**, **Morton GJ**. Leptin activates a novel CNS mechanism for insulin-independent normalization of
861 severe diabetic hyperglycemia. *Endocrinology* 152: 394–404, 2011. doi: 10.1210/en.2010-0890.

862 33. **Gloyn AL**, **Weedon MN**, **Owen KR**, **Turner MJ**, **Knight BA**, **Hitman G**, **Walker M**, **Levy JC**, **Sampson**
863 **M**, **Halford S**, **McCarthy MI**, **Hattersley AT**, **Frayling TM**. Large-scale association studies of variants
864 in genes encoding the pancreatic beta-cell KATP channel subunits Kir6.2 (KCNJ11) and SUR1
865 (ABCC8) confirm that the KCNJ11 E23K variant is associated with type 2 diabetes. *Diabetes* 52:
866 568–572, 2003. doi: 10.2337/diabetes.52.2.568.

867 34. **Glynn E**, **Thompson B**, **Vadrevu S**, **Lu S**, **Kennedy RT**, **Ha J**, **Sherman A**, **Satin LS**. Chronic Glucose
868 Exposure Systematically Shifts the Oscillatory Threshold of Mouse Islets: Experimental Evidence for
869 an Early Intrinsic Mechanism of Compensation for Hyperglycemia. *Endocrinology* 157: 611–623,
870 2016. doi: 10.1210/en.2015-1563.

871 35. **Goel P**. Insulin resistance or hypersecretion? The βIG picture revisited. *J Theor Biol* 384: 131–139,
872 2015. doi: 10.1016/j.jtbi.2015.07.033.

873 36. **Grespan E**, **Giorgino T**, **Arslanian S**, **Natali A**, **Ferrannini E**, **Mari A**. Defective Amplifying Pathway of
874 β-cell Secretory Response to Glucose in Type 2 Diabetes: Integrated Modeling of in vitro and in
875 vivo Evidence. .

876 37. **Ha J**, **Satin LS**, **Sherman AS**. A Mathematical Model of the Pathogenesis, Prevention, and Reversal of
877 Type 2 Diabetes. *Endocrinology* 157: 624–635, 2016. doi: 10.1210/en.2015-1564.

878 38. **Hardy T**, **Abu-Raddad E**, **Porksen N**, **De Gaetano A**. Evaluation of a mathematical model of diabetes
879 progression against observations in the Diabetes Prevention Program. *Am J Physiol Endocrinol*
880 *Metab* 303: E200-212, 2012. doi: 10.1152/ajpendo.00421.2011.

881 39. **Henquin JC**. Triggering and amplifying pathways of regulation of insulin secretion by glucose.
882 *Diabetes* 49: 1751–1760, 2000.

883 40. **Hulman A**, **Witte DR**, **Vistisen D**, **Balkau B**, **Dekker JM**, **Herder C**, **Hatunic M**, **Konrad T**, **Færch K**,
884 **Manco M**. Pathophysiological Characteristics Underlying Different Glucose Response Curves: A
885 Latent Class Trajectory Analysis From the Prospective EGIR-RISC Study. *Diabetes Care* 41: 1740–
886 1748, 2018. doi: 10.2337/dc18-0279.

887 41. **Jones CN**, **Pei D**, **Staris P**, **Polonsky KS**, **Chen YD**, **Reaven GM**. Alterations in the glucose-stimulated
888 insulin secretory dose-response curve and in insulin clearance in nondiabetic insulin-resistant
889 individuals. *J Clin Endocrinol Metab* 82: 1834–1838, 1997. doi: 10.1210/jcem.82.6.3979.

890 42. **Jung S-H**, **Jung C-H**, **Reaven GM**, **Kim SH**. Adapting to insulin resistance in obesity: role of insulin
891 secretion and clearance. *Diabetologia* 61: 681–687, 2018. doi: 10.1007/s00125-017-4511-0.

892 43. **Karin O**, **Swisa A**, **Glaser B**, **Dor Y**, **Alon U**. Dynamical compensation in physiological circuits. *Mol*
893 *Syst Biol* 12: 886, 2016.

894 44. **Kim MK**, **Reaven GM**, **Kim SH**. Dissecting the relationship between obesity and hyperinsulinemia:
895 Role of insulin secretion and insulin clearance. *Obesity (Silver Spring)* 25: 378–383, 2017. doi:
896 10.1002/oby.21699.

897 45. **Knowler WC**, **Barrett-Connor E**, **Fowler SE**, **Hamman RF**, **Lachin JM**, **Walker EA**, **Nathan DM**,
898 **Diabetes Prevention Program Research Group**. Reduction in the incidence of type 2 diabetes with
899 lifestyle intervention or metformin. *N Engl J Med* 346: 393–403, 2002. doi:
900 10.1056/NEJMoa012512.

901 46. **Kodama K**, **Tojjar D**, **Yamada S**, **Toda K**, **Patel CJ**, **Butte AJ**. Ethnic differences in the relationship
902 between insulin sensitivity and insulin response: a systematic review and meta-analysis. *Diabetes*
903 *Care* 36: 1789–1796, 2013. doi: 10.2337/dc12-1235.

904 47. **Koster JC**, **Remedi MS**, **Dao C**, **Nichols CG**. ATP and sulfonylurea sensitivity of mutant ATP-sensitive
905 K+ channels in neonatal diabetes: implications for pharmacogenomic therapy. *Diabetes* 54: 2645–
906 2654, 2005. doi: 10.2337/diabetes.54.9.2645.

907 48. **Lim EL**, **Hollingsworth KG**, **Aribisala BS**, **Chen MJ**, **Mathers JC**, **Taylor R**. Reversal of type 2 diabetes:
908 normalisation of beta cell function in association with decreased pancreas and liver triacylglycerol.
909 *Diabetologia* 54: 2506–2514, 2011. doi: 10.1007/s00125-011-2204-7.

910 49. **Mari A**, **Ferrannini E**. Beta-cell function assessment from modelling of oral tests: an effective
911 approach. *Diabetes Obes Metab* 10 Suppl 4: 77–87, 2008. doi: 10.1111/j.1463-1326.2008.00946.x.

912 50. **Mason CC**, **Hanson RL**, **Knowler WC**. Progression to type 2 diabetes characterized by moderate then
913 rapid glucose increases. *Diabetes* 56: 2054–2061, 2007. doi: 10.2337/db07-0053.

914 51. **Meigs JB**, **Muller DC**, **Nathan DM**, **Blake DR**, **Andres R**, **Baltimore Longitudinal Study of Aging**. The
915 natural history of progression from normal glucose tolerance to type 2 diabetes in the Baltimore
916 Longitudinal Study of Aging. *Diabetes* 52: 1475–1484, 2003.

917 52. **Morton GJ**, **Matsen ME**, **Bracy DP**, **Meek TH**, **Nguyen HT**, **Stefanovski D**, **Bergman RN**, **Wasserman**
918 **DH**, **Schwartz MW**. FGF19 action in the brain induces insulin-independent glucose lowering. *J Clin*
919 *Invest* 123: 4799–4808, 2013. doi: 10.1172/JCI70710.

920 53. **Nichols CG**, **Remedi MS**. The diabetic β-cell: hyperstimulated vs. hyperexcited. *Diabetes Obes Metab*
921 14: 129–135, 2012. doi: 10.1111/j.1463-1326.2012.01655.x.

922 54. **Nyman E**, **Rozendaal YJW**, **Helmlinger G**, **Hamrén B**, **Kjellsson MC**, **Strålfors P**, **van Riel NAW**,
923 **Gennemark P**, **Cedersund G**. Requirements for multi-level systems pharmacology models to reach
924 end-usage: the case of type 2 diabetes. *Interface Focus* 6: 20150075, 2016. doi:
925 10.1098/rsfs.2015.0075.

926 55. **Odgerel Z**, **Lee HS**, **Erdenebileg N**, **Gandbold S**, **Luvsanjamba M**, **Sambuughin N**, **Sonomtseren S**,
927 **Sharavdorj P**, **Jodov E**, **Altaisaikhan K**, **Goldfarb LG**. Genetic variants in potassium channels are
928 associated with type 2 diabetes in a Mongolian population. *J Diabetes* 4: 238–242, 2012. doi:
929 10.1111/j.1753-0407.2011.00177.x.

930 56. **Omar-Hmeadi M**, **Lund P-E**, **Gandasi NR**, **Tengholm A**, **Barg S**. Paracrine control of α-cell glucagon
931 exocytosis is compromised in human type-2 diabetes. *Nat Commun* 11: 1896, 2020. doi:
932 10.1038/s41467-020-15717-8.

933 57. **Perreault L**, **Bergman BC**, **Playdon MC**, **Dalla Man C**, **Cobelli C**, **Eckel RH**. Impaired fasting glucose
934 with or without impaired glucose tolerance: progressive or parallel states of prediabetes? *Am J*
935 *Physiol Endocrinol Metab* 295: E428-435, 2008. doi: 10.1152/ajpendo.90354.2008.

936 58. **Perry RJ**, **Camporez J-PG**, **Kursawe R**, **Titchenell PM**, **Zhang D**, **Perry CJ**, **Jurczak MJ**, **Abudukadier A**,
937 **Han MS**, **Zhang X-M**, **Ruan H-B**, **Yang X**, **Caprio S**, **Kaech SM**, **Sul HS**, **Birnbaum MJ**, **Davis RJ**, **Cline**
938 **GW**, **Petersen KF**, **Shulman GI**. Hepatic acetyl CoA links adipose tissue inflammation to hepatic
939 insulin resistance and type 2 diabetes. *Cell* 160: 745–758, 2015. doi: 10.1016/j.cell.2015.01.012.

940 59. **Petersen MC**, **Shulman GI**. Mechanisms of Insulin Action and Insulin Resistance. *Physiol Rev* 98:
941 2133–2223, 2018. doi: 10.1152/physrev.00063.2017.

942 60. **Piccinini F**, **Dalla Man C**, **Vella A**, **Cobelli C**. A Model for the Estimation of Hepatic Insulin Extraction
943 After a Meal. *IEEE Transactions on Biomedical Engineering* 63: 1925–1932, 2016. doi:
944 10.1109/TBME.2015.2505507.

945 61. **Piccinini F**, **Polidori DC**, **Gower BA**, **Bergman RN**. Hepatic but Not Extrahepatic Insulin Clearance Is
946 Lower in African American Than in European American Women. *Diabetes* 66: 2564–2570, 2017.
947 doi: 10.2337/db17-0413.

948 62. **Piller C**. Dubious diagnosis. *Science* 363: 1026–1031, 2019. doi: 10.1126/science.363.6431.1026.

949 63. **Polidori D**, **Bergman RN**, **Sumner AE**. A New Model-Based Method for Estimating Hepatic and
950 Peripheral Insulin Clearance from Intravenous Glucose Tolerance Test Data (2015 ADA abstract
951 254-LB). [date unknown].

952 64. **Porat S**, **Weinberg-Corem N**, **Tornovsky-Babaey S**, **Schyr-Ben-Haroush R**, **Hija A**, **Stolovich-Rain M**,
953 **Dadon D**, **Granot Z**, **Ben-Hur V**, **White P**, **Girard CA**, **Karni R**, **Kaestner KH**, **Ashcroft FM**, **Magnuson**
954 **MA**, **Saada A**, **Grimsby J**, **Glaser B**, **Dor Y**. Control of pancreatic β cell regeneration by glucose
955 metabolism. *Cell Metab* 13: 440–449, 2011. doi: 10.1016/j.cmet.2011.02.012.

956 65. **Pories WJ**, **Dohm GL**. Diabetes: have we got it all wrong? Hyperinsulinism as the culprit: surgery
957 provides the evidence. *Diabetes Care* 35: 2438–2442, 2012. doi: 10.2337/dc12-0684.

958 66. **Rahier J**, **Guiot Y**, **Goebbels RM**, **Sempoux C**, **Henquin JC**. Pancreatic beta-cell mass in European
959 subjects with type 2 diabetes. *Diabetes Obes Metab* 10 Suppl 4: 32–42, 2008. doi: 10.1111/j.1463-
960 1326.2008.00969.x.

961 67. **Ribbing J**, **Hamrén B**, **Svensson MK**, **Karlsson MO**. A model for glucose, insulin, and beta-cell
962 dynamics in subjects with insulin resistance and patients with type 2 diabetes. *J Clin Pharmacol* 50:
963 861–872, 2010. doi: 10.1177/0091270009349711.

964 68. **RISE Consortium**. Lack of Durable Improvements in β-Cell Function Following Withdrawal of
965 Pharmacological Interventions in Adults With Impaired Glucose Tolerance or Recently Diagnosed
966 Type 2 Diabetes. *Diabetes Care* 42: 1742–1751, 2019. doi: 10.2337/dc19-0556.

967 69. **Saisho Y**, **Butler AE**, **Manesso E**, **Elashoff D**, **Rizza RA**, **Butler PC**. β-cell mass and turnover in
968 humans: effects of obesity and aging. *Diabetes Care* 36: 111–117, 2013. doi: 10.2337/dc12-0421.

969 70. **Sedaghat AR**, **Sherman A**, **Quon MJ**. A mathematical model of metabolic insulin signaling pathways.
970 *Am J Physiol Endocrinol Metab* 283: E1084-1101, 2002. doi: 10.1152/ajpendo.00571.2001.

971 71. **Shanik MH**, **Xu Y**, **Skrha J**, **Dankner R**, **Zick Y**, **Roth J**. Insulin resistance and hyperinsulinemia: is
972 hyperinsulinemia the cart or the horse? *Diabetes Care* 31 Suppl 2: S262-268, 2008. doi:
973 10.2337/dc08-s264.

974 72. **Sharma AX**, **Quittner-Strom EB**, **Lee Y**, **Johnson JA**, **Martin SA**, **Yu X**, **Li J**, **Lu J**, **Cai Z**, **Chen S**, **Wang**
975 **M-Y**, **Zhang Y**, **Pearson MJ**, **Dorn AC**, **McDonald JG**, **Gordillo R**, **Yan H**, **Thai D**, **Wang ZV**, **Unger RH**,
976 **Holland WL**. Glucagon Receptor Antagonism Improves Glucose Metabolism and Cardiac Function
977 by Promoting AMP-Mediated Protein Kinase in Diabetic Mice. *Cell Rep* 22: 1760–1773, 2018. doi:
978 10.1016/j.celrep.2018.01.065.

979 73. **Tabák AG**, **Jokela M**, **Akbaraly TN**, **Brunner EJ**, **Kivimäki M**, **Witte DR**. Trajectories of glycaemia,
980 insulin sensitivity, and insulin secretion before diagnosis of type 2 diabetes: an analysis from the
981 Whitehall II study. *Lancet* 373: 2215–2221, 2009. doi: 10.1016/S0140-6736(09)60619-X.

982 74. **Thomas DD**, **Corkey BE**, **Istfan NW**, **Apovian CM**. Hyperinsulinemia: An Early Indicator of Metabolic
983 Dysfunction. *J Endocr Soc* 3: 1727–1747, 2019. doi: 10.1210/js.2019-00065.

984 75. **Topp B**, **Promislow K**, **deVries G**, **Miura RM**, **Finegood DT**. A model of beta-cell mass, insulin, and
985 glucose kinetics: pathways to diabetes. *J Theor Biol* 206: 605–619, 2000. doi:
986 10.1006/jtbi.2000.2150.

987 76. **Tricò D**, **Galderisi A**, **Mari A**, **Polidori D**, **Galuppo B**, **Pierpont B**, **Samuels S**, **Santoro N**, **Caprio S**.
988 Intrahepatic fat, irrespective of ethnicity, is associated with reduced endogenous insulin clearance
989 and hepatic insulin resistance in obese youths: a cross-sectional and longitudinal study from the
990 Yale Pediatric NAFLD cohort. .

991 77. **Utumatwishima JN**, **Chung ST**, **Bentley AR**, **Udahogora M**, **Sumner AE**. Reversing the tide - diagnosis
992 and prevention of T2DM in populations of African descent. *Nat Rev Endocrinol* 14: 45–56, 2018.
993 doi: 10.1038/nrendo.2017.127.

994 78. **Wang G**. Raison d'être of insulin resistance: the adjustable threshold hypothesis. *J R Soc Interface*
995 11: 20140892, 2014. doi: 10.1098/rsif.2014.0892.

996 79. **Wang Y-F**, **Khan M**, **van den Berg HA**. Interaction of fast and slow dynamics in endocrine control
997 systems with an application to β-cell dynamics. *Math Biosci* 235: 8–18, 2012. doi:
998 10.1016/j.mbs.2011.10.003.

999 80. **Wewer Albrechtsen NJ**, **Pedersen J**, **Galsgaard KD**, **Winther-Sørensen M**, **Suppli MP**, **Janah L**,
1000 **Gromada J**, **Vilstrup H**, **Knop FK**, **Holst JJ**. The Liver-α-Cell Axis and Type 2 Diabetes. *Endocr Rev* 40:
1001 1353–1366, 2019. doi: 10.1210/er.2018-00251.

1002 81. **Yki-Järvinen H**. Thiazolidinediones and the liver in humans. *Curr Opin Lipidol* 20: 477–483, 2009. doi:
1003 10.1097/MOL.0b013e3283321d37.

1004 82. **Zhu L**, **Dattaroy D**, **Pham J**, **Wang L**, **Barella LF**, **Cui Y**, **Wilkins KJ**, **Roth BL**, **Hochgeschwender U**,
1005 **Matschinsky FM**, **Kaestner KH**, **Doliba NM**, **Wess J**. Intra-islet glucagon signaling is critical for
1006 maintaining glucose homeostasis. *JCI Insight* 5, 2019. doi: 10.1172/jci.insight.127994.

1007

1008 **Figure Legends**

1009 Figure 1: IGT-first pathway to diabetes. (A) Assumed severe decline in peripheral insulin sensitivity. (B)
1010 Assumed mild decline in hepatic insulin sensitivity. (C) Simulated longitudinal changes based on the
1011 assumptions in (A) and (B) in fasting plasma glucose (FPG) and two-hour glucose (2hPG) during OGTTs
1012 performed at each time point. The virtual subject experiences first high two-hour glucose (IGT), then
1013 high fasting glucose (CGI), and finally crosses the 2hPG threshold for T2D. (D) Simulated longitudinal
1014 changes in fasting plasma insulin (FPI) and two-hour insulin (2hPI) during the OGTTs. Insulin increases
1015 early on but decreases later. (E) The component of β-cell function represented by σ decreases
1016 progressively throughout. (F) The β-cell mass, β, first increases during prediabetes, then decreases after
1017 diabetes onset.

1018 Figure 2: Insulin resistance (same as Fig. 1) does not lead to diabetes if beta-cell function is sufficiently
1019 responsive. The γ-dynamics is made stronger than in Fig. 1 by decreasing γ_s to 90 *mg/dl* from 100 *mg/dl*
1020 (see other parameters in Table S12A). (A) Assumed severe decline in peripheral insulin sensitivity. (B)
1021 Assumed mild decline in hepatic insulin sensitivity. (C) Simulated longitudinal changes in FPG and 2hPG
1022 during OGTTs performed at each time point. The virtual subject experiences modest rises in glucose and
1023 crosses the threshold for IGT but never crosses the thresholds for IFG, CGI or T2D. (D) Simulated
1024 longitudinal changes in fasting plasma insulin (FPI) and two-hour insulin (2hPI) during the OGTTs.
1025 Insulin concentration increases and saturates but never declines. (E) The β-cell function component σ first
1026 decreases, but then levels off. Increase in the β-cell function component represented by γ (not shown)
1027 helps limit the rise in glucose, which allows the β-cell mass β to increase gradually throughout (F).

1028 Figure 3: IFG-first pathway to diabetes. (A) Assumed mild decline in peripheral insulin sensitivity. (B)
1029 Assumed severe decline in hepatic insulin sensitivity component $hepa_{SI}$. (C) Simulated longitudinal
1030 changes in FPG and 2hPG during OGTTs performed at each time point. The virtual subject experiences
1031 first high FPG (IFG), then high 2hPG (CGI), and finally crosses the FPG threshold for T2D first.
1032 Simulated longitudinal changes in fasting plasma insulin (FPI) and two-hour insulin (2hPI) during the
1033 OGTTs. Insulin concentration increases early on but decreases later. (E) The β-cell function component σ
1034 decreases progressively throughout. (F) The β-cell mass β increases during prediabetes then decreases
1035 after diabetes onset.

1036 Figure 4: The CGI state is not obligatory. (A), (B): Extreme discrepancy between peripheral and hepatic
1037 (A – B) insulin resistance results in progression directly from IGT to T2D without passing through CGI
1038 based on OGTTs performed at each time point (C). FPG does not exceed the threshold for IFG until after
1039 T2D onset. (D) Simulated longitudinal changes in fasting plasma insulin (FPI) and two-hour insulin
1040 (2hPI) during the OGTTs. Insulin increases early on, then decreases. (E) The β-cell function component σ
1041 decreases more rapidly than in Figs. 1, 3. (F) The β-cell mass β increases during prediabetes, then
1042 decreases after diabetes onset.

1043 Figure 5: (A) Two-hour glucose (2hPG) plotted vs. fasting glucose (FPG) for varying degrees of
1044 peripheral insulin sensitivity, S_I, and hepatic insulin sensitivity $hepa_{SI}$, starting from the same initial
1045 values as in Figs. 1 – 4 and evolving to the target values, tar_{SI} (Eq. A13) and tar_{hepaSI} (Eq. A14) as
1046 follows: from upper left to lower right, the tar_{SI} values increase: 0.1, 0.17, 0.22, 0.33, 0.4 and 0.5; and the

tar_{hepaSI} values decrease: 0.85, 0.6, 0.45, 0.35, 0.25 and 0.1. All other parameters are fixed. (B) expanded view of (A) to highlight the prediabetes region.

Figure 6: Glucose during OGTTs performed at the times indicated by the black dots in (A) Fig. 1 (IGT-first pathway) and (B) Fig. 3 (IFG-first pathway). (C, D) insulin corresponding to A and B, respectively. See text for details.

Figure 7: Insulin during IVGTTs performed at the time points indicated by the black dots in (A) Fig. 1 (IGT-first pathway) and (B) Fig. 3 (IFG-first pathway). (C, D): RRP size (numbers of vesicles) corresponding to A and B, respectively. Decline of AIRg parallels the reduction of RRP for each case.

Figure 8: Drug therapies targeting either peripheral insulin sensitivity (modeled as a rapid increase in S_I) or hepatic insulin sensitivity (modeled as a rapid increase in $hepa_{SI}$; see Tables S13 – S16 for details). The drugs are applied in the early stages of T2D (A, B) or during prediabetes (C, D). (A, C) Dominant peripheral insulin resistance, leading to IGT-first pathway as in Fig. 1. (B, D) Dominant hepatic insulin resistance, leading to IFG-first pathway as in Fig. 3. The appropriately targeted drug is more effective than the inappropriately targeted drug in each case, but therapy is more effective when initiated during prediabetes.

Figure 9: Effects of insulin clearance and insulin-induced insulin resistance. The case of Fig. 1 (IGT first) is re-simulated with varying rates of insulin clearance and induced insulin resistance, defined by Eqs. 13 – 16. Panel A: $S_I = S_{I,0}E$, where $S_{I,0}$ is calculated as in Fig. 1 and E is the induced effect plotted in Panel F. Legend: *black* (control), same as Fig. 1, but with insulin clearance k = 0.4861 min^{-1}, essentially no induced effect (α_E = 300 μU/ml); *green*: reduced clearance (k = 0.37499 min^{-1}), modest induced effect (α_E = 50 μU/ml); *blue*: k = 0.37499 min^{-1}, stronger induced effect (α_E = 15 μU/ml); *red*: k = 0.37499 min^{-1}, very strong induced effect (α_E = 5 μU/ml). Other parameters are listed in Table S17.

Fig. 1

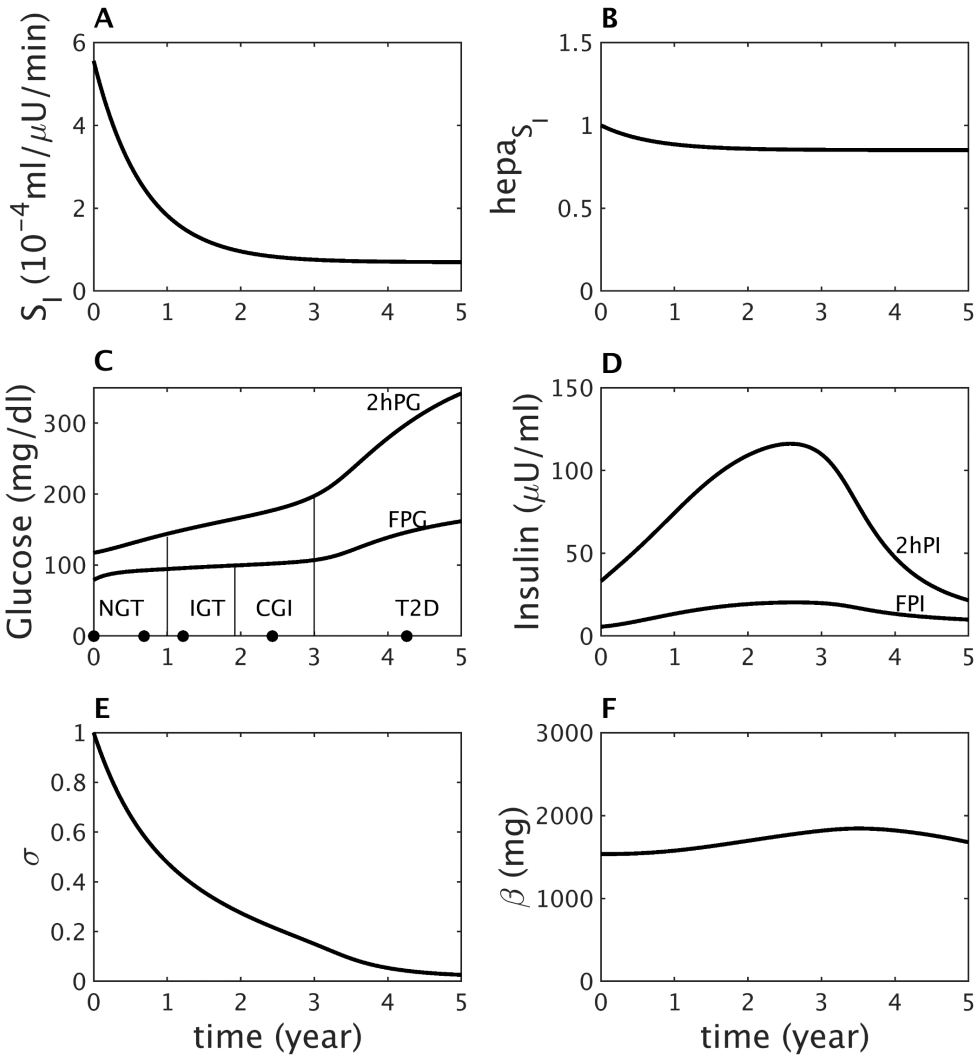
A
S_I (10^{-4}ml/μU/min)
B
hepa$_{S_I}$
C
Glucose (mg/dl)
2hPG
FPG
NGT
IGT
CGI
T2D
D
Insulin (μU/ml)
2hPI
FPI
E
σ
F
β (mg)
time (year)
time (year)

Fig. 2

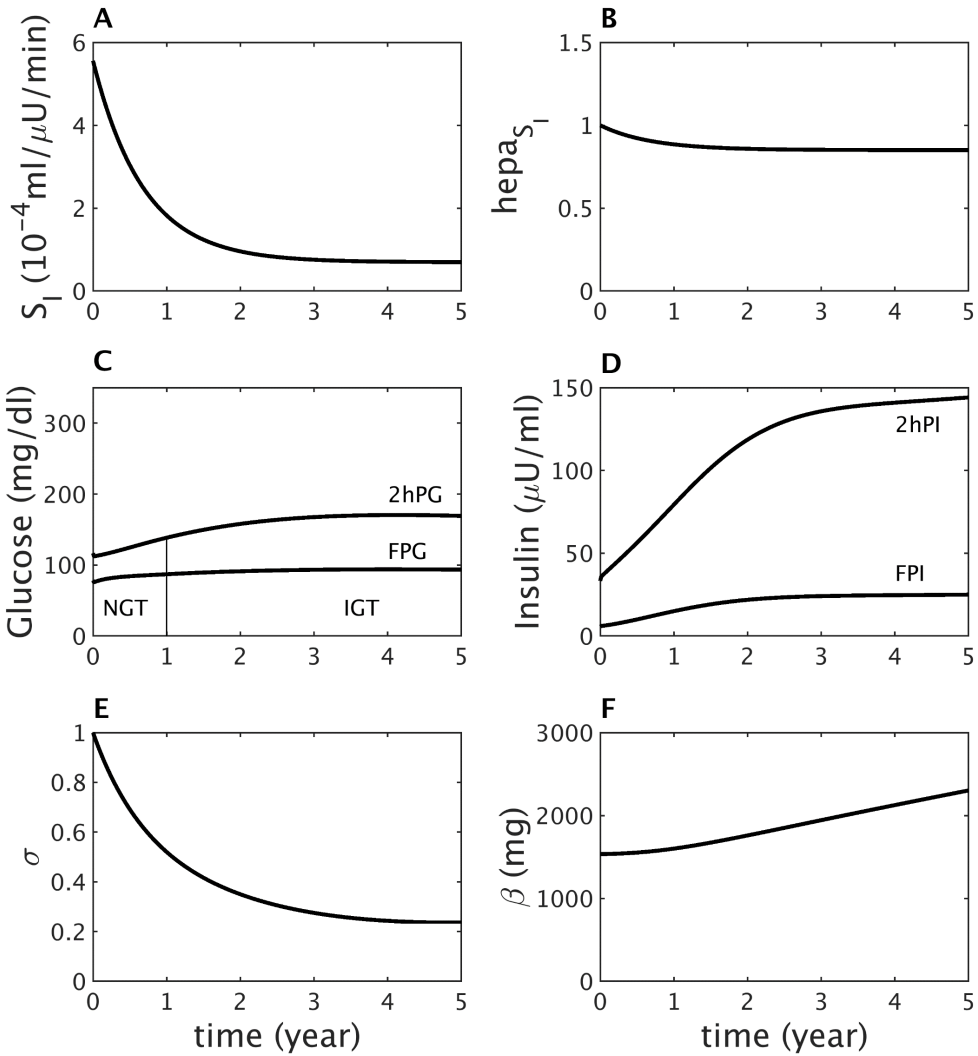
A
S_I (10^{-4}ml/μU/min)
B
$hepa_{S_I}$
C
Glucose (mg/dl)
2hPG
FPG
NGT
IGT
D
Insulin (μU/ml)
2hPI
FPI
E
σ
F
β (mg)
time (year)
time (year)

Fig. 3

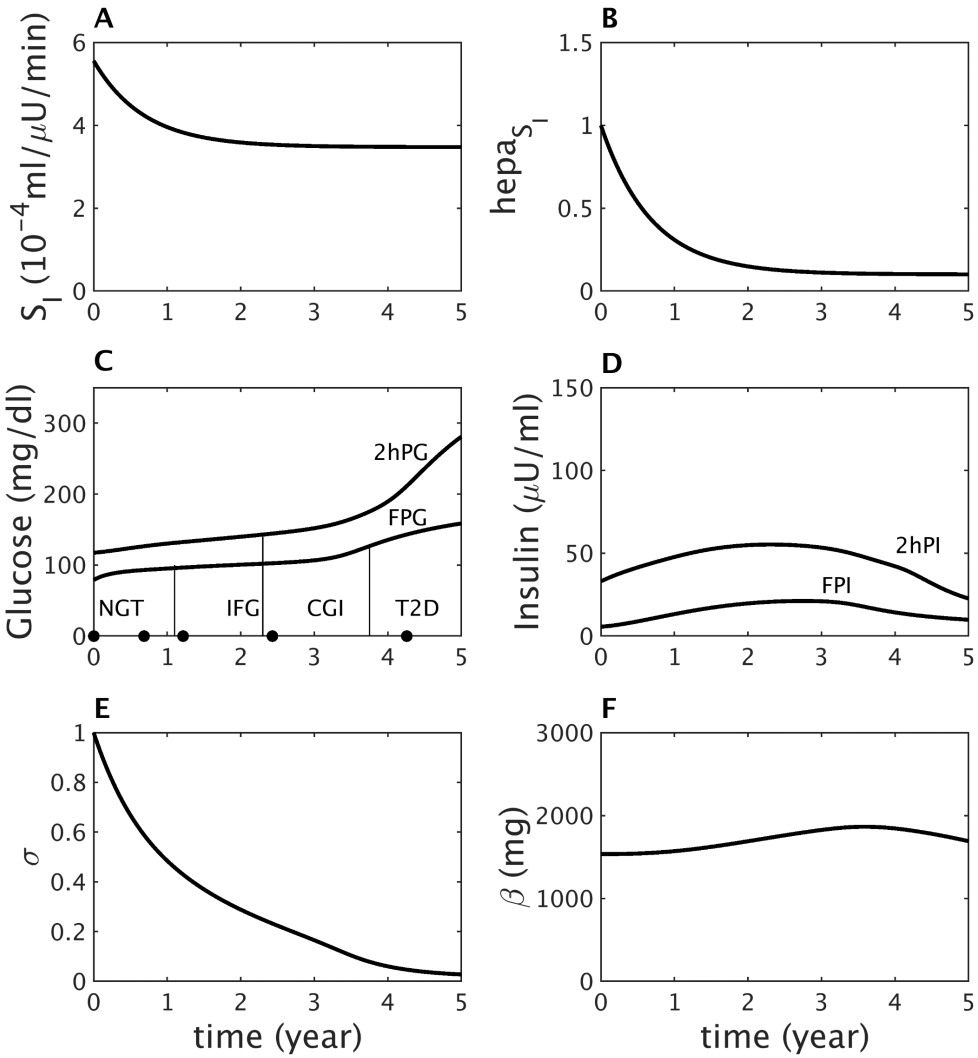
A
S_I (10^{-4}ml/μU/min)
B
hepa$_{S_I}$
C
Glucose (mg/dl)
2hPG
FPG
NGT
IFG
CGI
T2D
D
Insulin (μU/ml)
2hPI
FPI
E
σ
F
β (mg)
time (year)
time (year)

Fig. 4

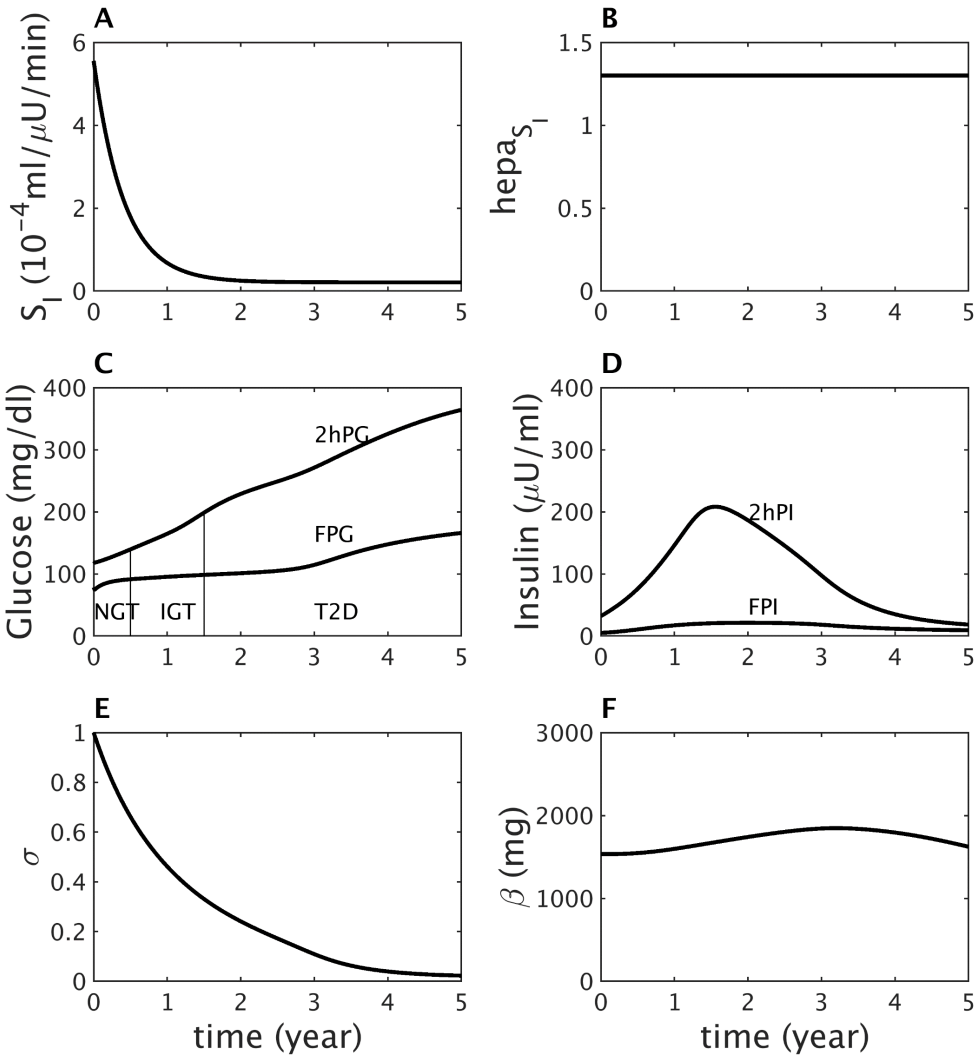
A
S_I (10^{-4}ml/μU/min)
B
$hepa_{S_I}$
C
Glucose (mg/dl)
2hPG
FPG
NGT
IGT
T2D
D
Insulin (μU/ml)
2hPI
FPI
E
σ
F
β (mg)
time (year)
time (year)

Fig. 5

A

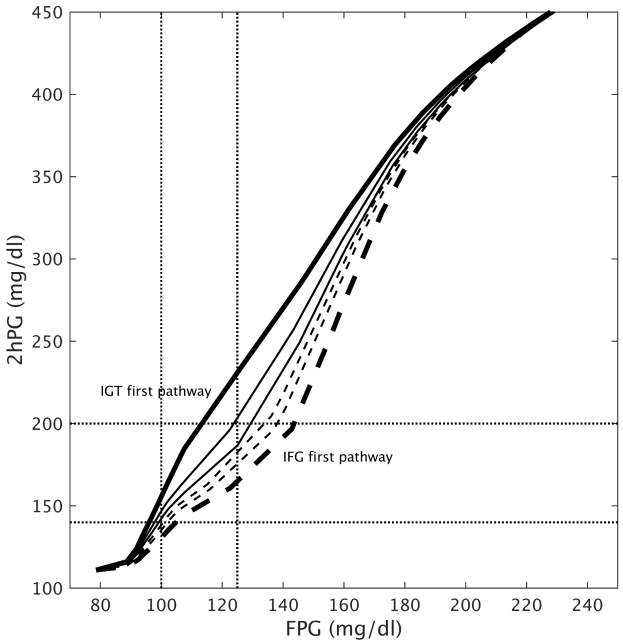
450
400
350
300
250
200
150
100
2hPG (mg/dl)
80
100
120
140
160
180
200
220
240
FPG (mg/dl)
IGT first pathway
IFG first pathway

B

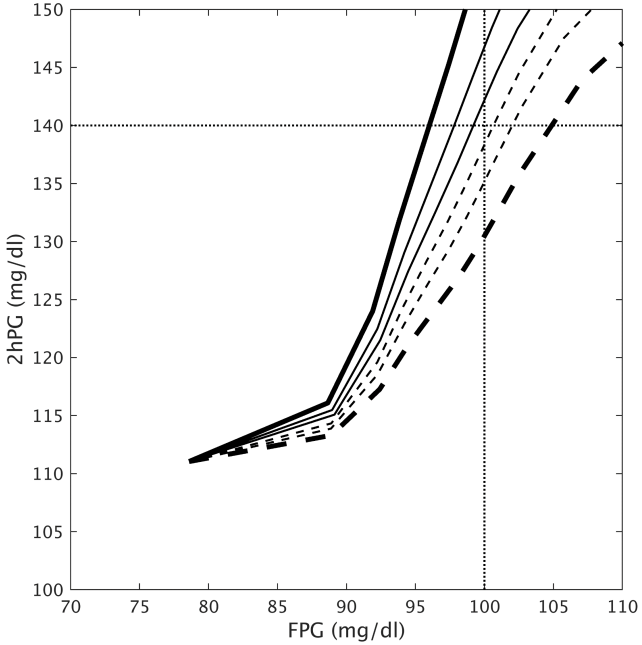
150
145
140
135
130
125
120
115
110
105
100
2hPG (mg/dl)
70
75
80
85
90
95
100
105
110
FPG (mg/dl)

Fig. 6

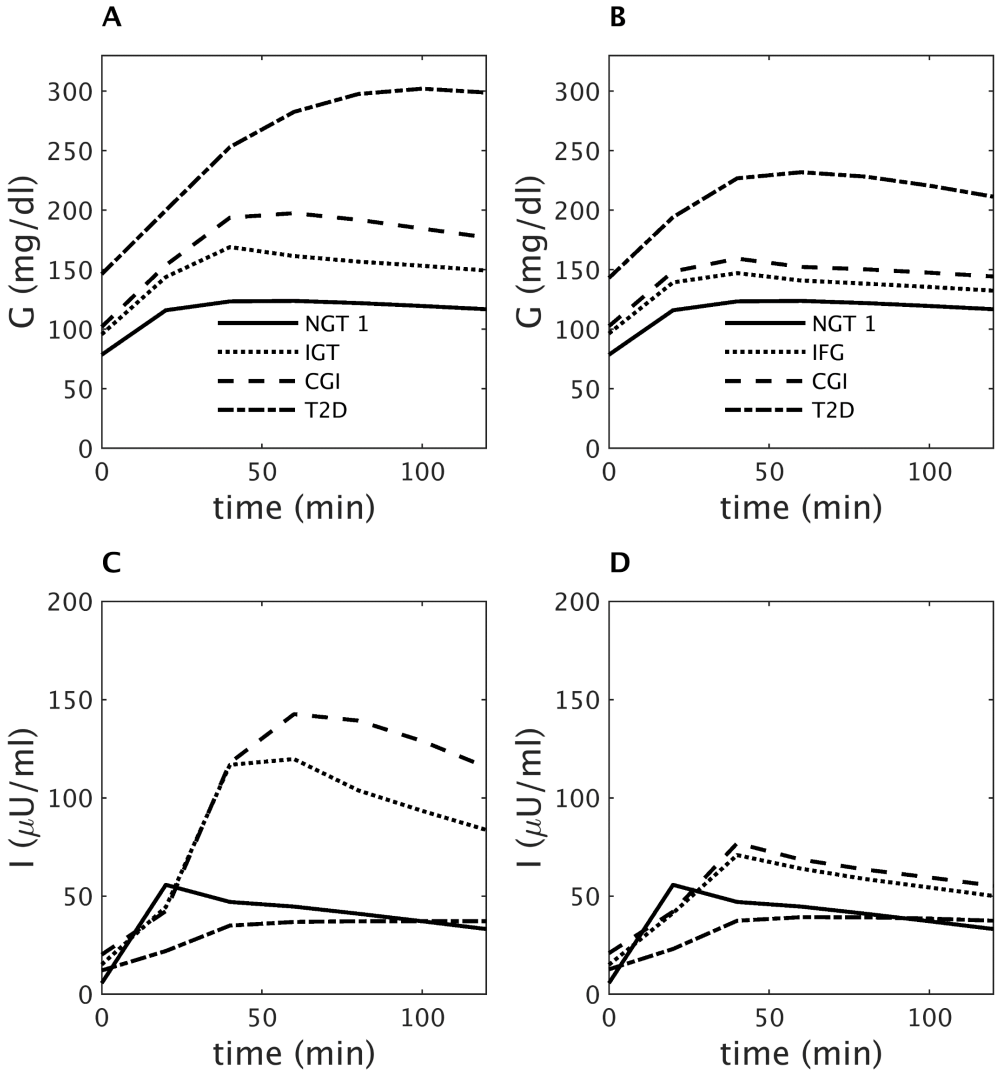
A
B
C
D
G (mg/dl)
I (μU/ml)
time (min)
NGT 1
IGT
IFG
CGI
T2D
0
50
100
150
200
250
300

Fig. 7

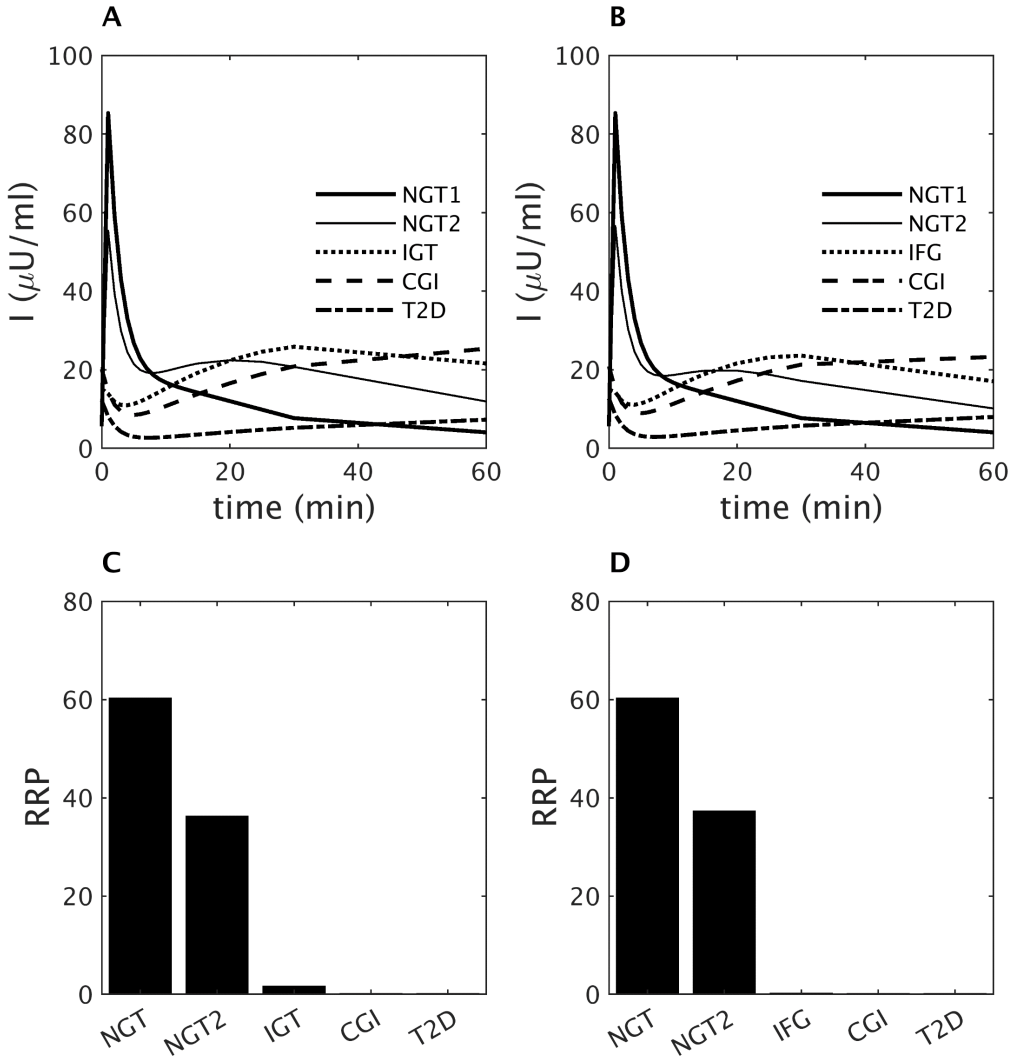
A
B
C
D
I (μU/ml)
time (min)
NGT1
NGT2
IGT
IFG
CGI
T2D
RRP
NGT
NGT2
IGT
IFG
CGI
T2D
0
20
40
60
80
100

Fig. 8

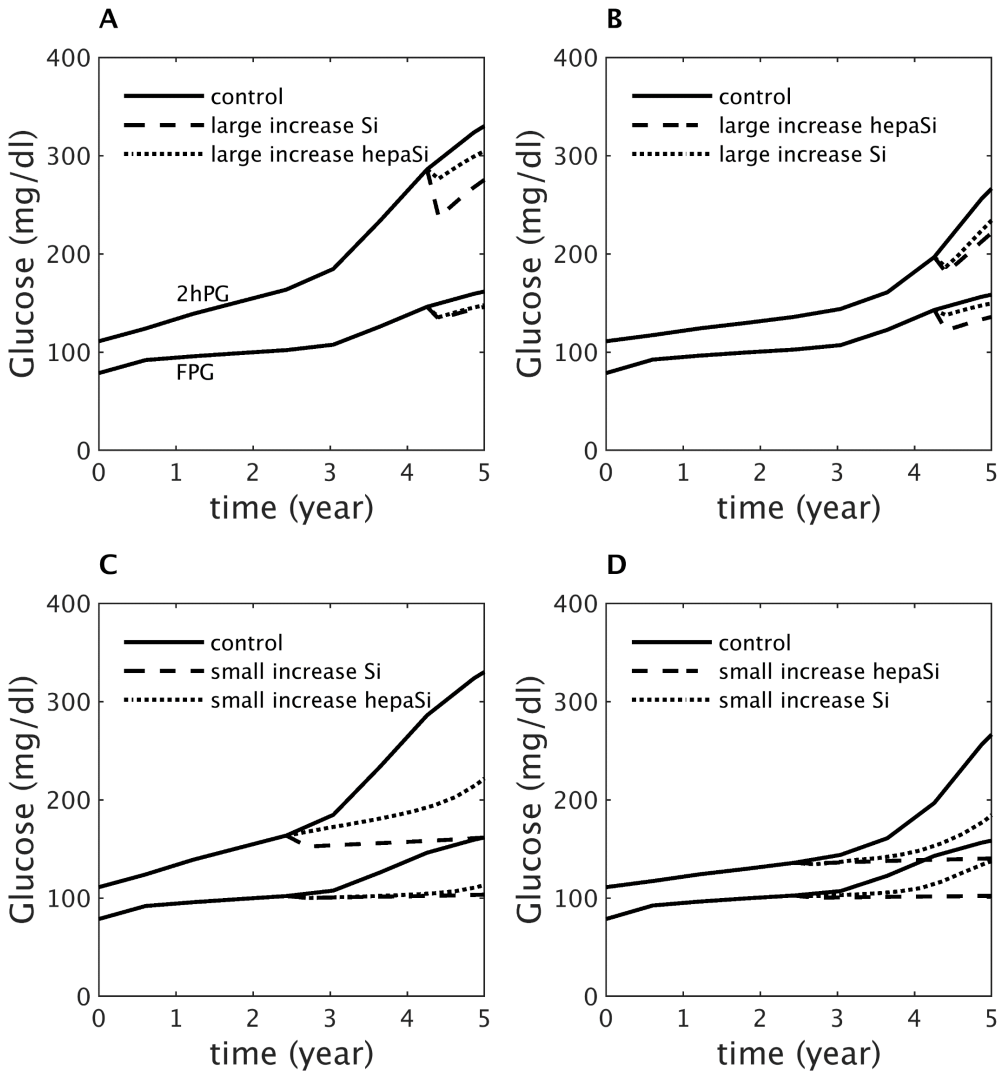
A
B
C
D
Glucose (mg/dl)
time (year)
control
large increase Si
large increase hepaSi
2hPG
FPG
large increase hepaSi
small increase Si
small increase hepaSi
0
100
200
300
400
0
1
2
3
4
5

Fig. 9

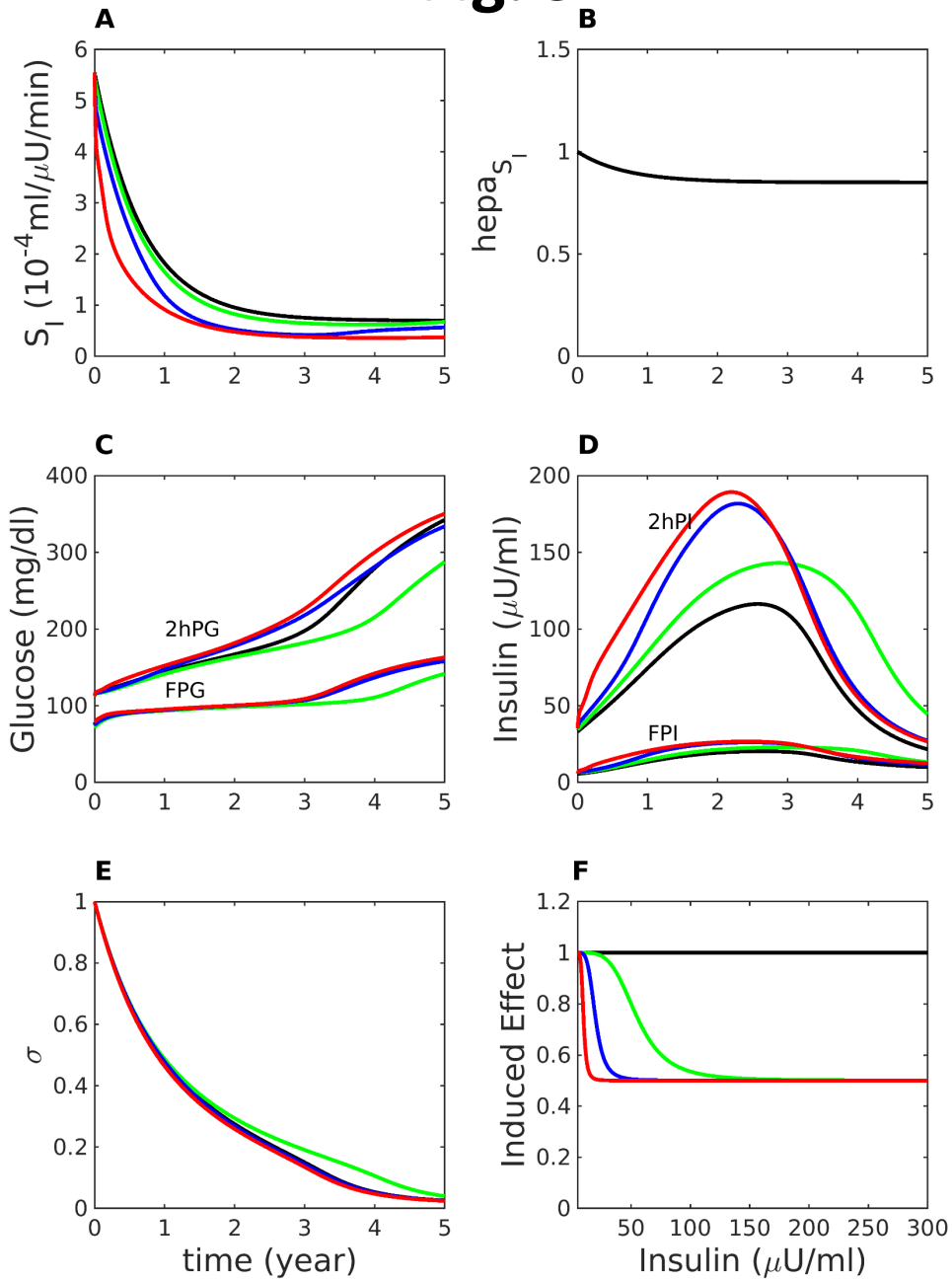
A
B
C
D
E
F
S_I (10^{-4}ml/μU/min)
$hepa_{S_I}$
Glucose (mg/dl)
2hPG
FPG
Insulin (μU/ml)
2hPI
FPI
σ
time (year)
Induced Effect
Insulin (μU/ml)